Quantum-mechanical study of nonreactive collisions between Rb($5\,^2P$) and H_2 or D_2 ($^1\Sigma_g^+, v=0$)

J. Pascale, F. Rossi, and W. E. Baylis*
Institut de Recherche Fondamentale, Service de Physique des Atomes et des Surfaces, Centre d'Etudes Nucléaires de Saclay, 91191 Gif-Sur-Yvette Cedex, France
(Received 23 March 1987)

Close-coupling quantum-mechanical calculations have been carried out in the rigid-rotor approximation for low-energy collisions ($E \lesssim 0.3$ eV) of Rb($5\,^2P_{j_1}$) with H_2 or $D_2(j_2)$, the molecule lying in its ground electronic and vibrational state. The calculations use realistic adiabatic potential energy surfaces which are determined from previous pseudopotential calculations, and the main nonadiabatic coupling matrix elements involved during the collision are evaluated. The total cross sections for various transitions among the $5\,^2P_{j_1}$ fine-structure levels of Rb and rotational levels $j_2=0,2,4$, and $j_2=1,3$ of the molecule are determined and discussed. The results are in good agreement with crossed-beam experimental data concerning the $5\,^2P_{1/2}\rightarrow 5\,^2P_{3/2}$ transition in Rb induced by collisions with H_2 or D_2.

I. INTRODUCTION

Collisional quenching from the first $n\,^2P$ level to the ground state of an alkali-metal atom A by a molecular perturber M has been intensively studied in the past (see recent reviews of Refs. 1 and 2). In particular, much theoretical efforts have been expanded to understand the main nonadiabatic coupling mechanisms responsible for the quenching processes,[3,4] and recent developments in theoretical methods lead now to detailed comparisons between theory and experiment.[5] Comparatively, intra-$n\,^2P$ transitions in A resulting from thermal to suprathermal collisions with M have been the subject of numerous experimental studies (see Refs. 6–11 and references therein), but only very few theoretical works have been devoted to the dynamics of these processes.[7,12–14] As a result, the interpretations of experimental data concerning these processes remain mostly qualitative or incomplete. In a recent study[13,14] a semiclassical model has been proposed, where the molecular perturber (H_2 or N_2) is treated as a structureless particle. As discussed elsewhere,[15] in this model we consider an electronic Hamiltonian which is independent of the orientation of the molecular perturber, and which is thus invariant under the symmetry group C_{2v} instead of the symmetry group C_s. Then the problem of the collision between $A(n\,^2P)$ and M reduces to coupling between three adiabatic molecular states with energies which have been evaluated from the adiabatic potential energy curves of the equivalent A–rare-gas system and the quadrupole moment of M. From this model, two nonadiabatic coupling mechanisms have been clearly identified, which may compete with each other for inducing fine-structure transitions.[13,14] As discussed elsewhere for $A(n\,^2P)$ + rare-gas collisions,[16] these nonadiabatic couplings result from spin-orbit decoupling of molecular states during the collision. As in the case of $A(n\,^2P)$ + rare-gas collisions, a first nonadiabatic coupling occurs at intermediate distances R between the A core and the center of mass of M, namely, at $R \simeq 10-15$ a.u. (atomic units). A second nonadiabatic coupling occurs at shorter distances ($R \simeq 5-7$ a.u.) because of the anisotropy of the molecular perturber. It was shown[13,14] that this second nonadiabatic coupling accounts for the large enhancement of the cross section for the $5\,^2P_{1/2}\rightarrow 5\,^2P_{3/2}$ transition in Rb when the perturber is changed from He to H_2 as it was experimentally observed.[9] However, this model cannot explain the large isotopic effect which was observed in a Rb($5\,^2P$)+H_2,D_2 crossed-beam experiment[10] where the relative collision energy of the system and the rotational temperature $T_{\rm rot}$ of the molecule were varied independently: in this experiment it was found that for D_2 the fine-structure transition cross section exhibits a strong dependence on $T_{\rm rot} \lesssim 300$ K, suggesting that the rotational levels of D_2 are playing an important role during the collision. Obviously, the rotational levels of M cannot be taken into account in the model discussed above. In order to explain the experimental data of Ref. 10, it is necessary that the cross sections for transitions among the $5\,^2P_{j_1}$ levels of Rb and rotational levels j_2 of M be determined, and that the rotational population distribution of M be considered. Since thermal to suprathermal energies are regarded, it is therefore appropriate to perform three-dimensional close-coupling quantum-mechanical calculations similar to those carried out in the case of $F(^2P)+H_2$, D_2 (Refs. 17 and 18), and $C^+(^2P)+H_2$ collisions.[19]

In a preceding paper[20] we have developed a general formulation of the close-coupling quantum-mechanical treatment of nonreactive collisions between two structured systems. It is applied in this paper for studying the processes

$$\mathrm{Rb}(5\,^2P_{j_1})+M(j_2)\rightarrow \mathrm{Rb}(5\,^2P_{j_1'})+M(j_2')-\Delta E\ , \quad (1)$$

where Rb is excited in the $5\,^2P_{1/2}$ or $5\,^2P_{3/2}$ level and M is H_2 or D_2 in its ground electronic and vibrational state, and in a rotational level j_2. The method treats M as a rigid rotor and is based on the expansion of the three-body interaction describing the Rb-M system in terms of spherical harmonics. It is briefly outlined in Sec. II A, where the main formulas for the close-coupling calcula-

tions are given in a space-fixed coordinate frame. The procedure for evaluating the expansion coefficients of the Rb-M interaction from previous pseudopotential molecular-structure calculations—performed for the symmetry groups $C_{\infty v}$ and C_{2v} (Ref. 21)—is given in Sec. II B. This determines the coupling matrix elements of the close-coupling formalism. It is shown in Sec. II C that in the close-coupling calculations our method uses implicitly realistic adiabatic potential energy surfaces associated with the $5\,^2P_{j_1}$ levels of Rb. Then, the main nonadiabatic coupling matrix elements are explicitly evaluated (Sec. II D). Though the latter are unnecessary for the close-coupling calculations, they are very useful to understand better the coupling mechanisms responsible for processes (1). The results of the close-coupling calculations concerning the total cross sections of all the inelastic processes (1) are then presented and discussed in Sec. III. In a previous letter[22] the results concerning the $5\,^2P_{1/2}\rightarrow 5\,^2P_{3/2}$ transition in Rb induced by collisions with H_2 or D_2 were reported and discussed in relation with available experimental data.[6,10] These are discussed further in Sec. III. Finally, a summary and concluding remarks are given in Sec. IV.

II. THEORY

A. Formulation of the collision problem

The formulation of the collision between Rb($n\,^2P_{j_1}$) and M can be much reduced when the following approximations are considered. First, the Rb atom may be treated as a frozen-core A atom plus a valence electron e^-. Moreover, the molecule M may be assumed lying in its ground electronic and vibrational state $^1\Sigma_g^+$ ($v=0$) during the collision, its internuclear distance r_2 being fixed at its equilibrium value 1.4 a.u. (rigid-rotor approximation). Subsequently, r_2 will be ignored in the formulas. Then, the interaction between Rb and M is reduced to a three-body interaction $V(\mathbf{r}_1,\mathbf{R},\hat{\mathbf{r}}_2)$, where $\mathbf{r}_1$ and $\mathbf{R}$ denote, respectively, the position vectors of e^- and the center of mass of M with respect to A, and $\hat{\mathbf{r}}_2=\mathbf{r}_2/r_2$ specifies the orientation of the molecule. This approximation is consistent with our previous l-dependent semiempirical pseudopotential molecular-structure calculations of the A-H_2 systems,[21] which therefore can be used in the present study. Second, it is assumed that only the electronic molecular states of the Rb-M system associated asymptotically with the $5\,^2P_{1/2}$ and $5\,^2P_{3/2}$ levels of Rb are involved during the collision. This amounts to neglecting possible quenching to the ground state of Rb or electronic excitation to upper levels. In view of the relative collision energies considered in this study (less than about 0.3 eV), this approximation appears to be quite justified. In particular, our previous molecular-structure calculations[21] indicate that a crossing between the $X\,^2A_1$ and $A\,^2B_2$ potential energy curves occurs at $R\simeq 2.6$ a.u. and about 16 eV above the $5\,^2P$ level of Rb. This suggests that quenching from the $5\,^2P$ level of Rb to its ground state cannot affect significantly the fine-structure transition cross sections, even if stretching of M is envisaged.

The close-coupling quantum-mechanical formalism for processes (1) can be derived straightforwardly from our preceding paper[20] in which the inelastic scattering of two structured systems interacting through a three-body interaction is considered. We summarize hereafter the method and use the notations of Ref. 20. The method is an extension of that previously developed for studying $A(n\,^2P)$ + rare-gas collisions.[23] It is based first on the expansion of the A-M three-body interaction in terms of spherical harmonics. In a rotating coordinate frame with the quantization axis along $\mathbf{R}$, one has

$$V(\mathbf{r}_1,R,\hat{\mathbf{r}}_2)=4\pi\sum_{k_1,k_2,q} v_{k_1k_2q}(r_1,R)Y_{k_1q}(\hat{\mathbf{r}}_1)Y_{k_2-q}(\hat{\mathbf{r}}_2)\ . \tag{2}$$

The rotation and inversion symmetries of the system are fully exploited to reduce the number of coupled equations. In a space-fixed coordinate frame with quantization axis $\hat{\mathbf{z}}$ it is found that a convenient eigenfunction basis set with definite parity π_t can be built from eigenfunctions of j_1^2, j_2^2, j^2, l^2, J^2, and J_z. Here the total angular momentum $\mathbf{j}_1$ of e^- and the rotational angular momentum $\mathbf{j}_2$ of M are coupled with the orbital angular momentum $\boldsymbol{l}$ of the relative motion of the system through the intermediate angular momentum $\mathbf{j}=\mathbf{j}_1+\mathbf{j}_2$, to give the total angular momentum $\mathbf{J}=\mathbf{j}+\boldsymbol{l}$, with component J_z. Since only the $5\,^2P_{1/2}$ and $5\,^2P_{3/2}$ levels of Rb are considered in building the eigenfunction basis set, it can be noted that in expansion (2) of the three-body interaction, k_1 takes only the values 0 and 2. Moreover, because of the homonuclearity of M, k_2 can take only even values. The latter remark implies that for a given molecule (H_2 or D_2), only even (for para-H_2 or ortho-D_2) or odd (ortho-H_2 or para-D_2) rotational quantum numbers are coupled, reducing further the number of coupled equations. Then, for a given ortho or para molecule, the close-coupling equations for the radial motion of the system reduce, for a given total energy E of the system, to blocks of equations with given J and π_t values:

$$\left[\frac{d^2}{dR^2}+k_{12}'^2-\frac{l'(l'+1)}{R^2}\right]F^{J\pi_t}_{\alpha'l',\alpha l}(R,E) =2\mu\sum_{\alpha'',l''}V^J_{\alpha'l',\alpha''l''}(R)F^{J\pi_t}_{\alpha''l'',\alpha l}(R,E)\ , \tag{3}$$

where $J(J+1)$ is the eigenvalue of J^2. In Eq. (3) atomic units have been used; the unprimed labels correspond to the initial state and the single-primed labels correspond to the final state; α denotes the set of quantum numbers j_1, j_2, and j. Finally, the wave number k'_{12} of the relative motion of the system is defined as

$$k_{12}'^2=2\mu(E-E_{j_1'}-E_{j_2'})\ , \tag{4}$$

where μ is the reduced mass of the system, $E_{j_1'}$ is the energy of the $5\,^2P_{j_1'}$ level of Rb, and $E_{j_2'}$ is the rotational energy level of M. Hereafter, the energies will be rela-

tive to $E_{1/2}+E_0$ (for para-H_2 or ortho-D_2) or $E_{1/2}+E_1$ (for ortho-H_2 or para-D_2). The coupling matrix elements can be written in terms of $\bar{v}_{k_1k_2q}(R)$, the expectation value of $v_{k_1k_2q}(r_1,R)$ [see Eq. (2)] over the radial wave function of the $5\,^2P$ level of Rb, and in terms of 3-j, 6-j, and 9-j symbols (see Ref. 24, for example),

$$
\begin{aligned}
V^J_{\alpha' l',\alpha'' l''}(R)=&\sum_{\substack{k_1=0,2\\ k_2 \text{ even}}}\sum_{q=-\min(k_1,k_2)}^{\min(k_1,k_2)}\bar{v}_{k_1k_2q}(R)\\
&\times\sum_{k_3=|k_1-k_2|}^{k_1+k_2}(-1)^{j'_1+j'_2+J+1/2+l''+k_1+k_2}(2k_3+1)\\
&\times[(2k_1+1)(2k_2+1)(2j'_1+1)(2j'_2+1)\\
&\times(2j'+1)(2l'+1)(2j''_1+1)(2j''_2+1)(2j''+1)(2l''+1)]^{1/2}\\
&\times\begin{pmatrix} j'_1 & k_1 & j''_1\\ \frac{1}{2} & 0 & -\frac{1}{2}\end{pmatrix}\begin{pmatrix} j'_2 & k_2 & j''_2\\ 0 & 0 & 0\end{pmatrix}\begin{pmatrix} l' & k_3 & l''\\ 0 & 0 & 0\end{pmatrix}\\
&\times\begin{pmatrix} k_1 & k_2 & k_3\\ q & -q & 0\end{pmatrix}\begin{Bmatrix} l' & l'' & k_3\\ j'' & j' & J\end{Bmatrix}\begin{Bmatrix} j'_1 & j'_2 & j'\\ j''_1 & j''_2 & j''\\ k_1 & k_2 & k_3\end{Bmatrix},
\end{aligned}
\tag{5}
$$

with $\bar{v}_{k_1k_2-q}(R)=\bar{v}_{k_1k_2q}(R)$. Note that because of the parity, each value of J couples positive values of l and l' such that $|l-l'|$ is even.

Only the open channels have been included in the close-coupling calculations, and the rotational levels 0,2,4 (for para-H_2 and ortho-D_2), and 1,3 (for ortho-H_2 and para-D_2) have been considered. This corresponds to blocks of coupled equations, for given J and π_t values, of dimension up to 45 (for para-H_2 and ortho-D_2) or 30 (for ortho-H_2 and para-D_2). Given a relative energy E, the blocks of coupled equations for given J and π_t values are solved under normal boundary conditions by using the log-derivative method,[25] and the $T^{EJ\pi_t}_{(j'_1j'_2j'l';j_1j_2jl)}$ matrix is obtained. Then the total cross section for the transition from the initial state j_1j_2 to the final state $j'_1j'_2$ is defined as

$$
\sigma_{j'_1j'_2\leftarrow j_1j_2}(E)=\frac{\pi}{k_{12}^2}\frac{1}{(2j_1+1)(2j_2+1)}\times\sum_{\substack{J,l,l',\\ j,j',\pi_t}}(2J+1)\,|\,T^{EJ\pi_t}_{(j'_1j'_2j'l';j_1j_2jl)}\,|^2 . \tag{6}
$$

When analyzing the partial-wave contributions to the total cross section, it is useful sometimes to define an opacity function or probability $P_{j'_1j'_2\leftarrow j_1j_2}(E,l)$ as

$$
P_{j'_1j'_2\leftarrow j_1j_2}(E,l)=\frac{1}{(2j_1+1)(2j_2+1)(2l+1)}\times\sum_{\substack{Jl',\\ j,j',\pi_t}}(2J+1)\,|\,T^{EJ\pi_t}_{(j'_1j'_2j'l';j_1j_2jl)}\,|^2 . \tag{7}
$$

Then, replacing l by an impact parameter $b\simeq l/k_{12}$, one may write the total cross section in the familiar semiclassical form

$$
\sigma_{j'_1j'_2\leftarrow j_1j_2}(E)\simeq 2\pi\int_0^\infty P_{j'_1j'_2\leftarrow j_1j_2}(E,b)b\,db . \tag{8}
$$

B. Determination of coupling matrix elements

The determination of coupling matrix elements [see Eq. (5)] requires the knowledge of a limited number of coefficients $\bar{v}_{k_1k_2q}(R)$ since $k_1=0,2$, $j_2\le 4$ which implies k_2 to take values smaller or equal to 8, and $|q|=\min(k_1,k_2)$. The procedure used in this paper to evaluate the coefficients $\bar{v}_{k_1k_2q}(R)$ is similar to that previously developed for $A(n\,^2P)$ + rare-gas collisions[23] or for $C^+(n\,^2P)+H_2$ collisions.[26] However, an important improvement to the procedure has been made with respect to Ref. 26 as it will be shown later on. The pro-

cedure consists in diagonalizing the total Hamiltonian $H=H_0+V$ in the atomic basis set restricted to the $n\,^2P$ level, where H_0 is the Hamiltonian of the isolated Rb atom, and where V is replaced by an effective three-body interaction $\tilde{V}$ in order to account for coupling with other nl levels (see discussion of the preceding paper[20]). Equivalently, this comes to replace the coefficients $\bar{v}_{k_1k_2q}(R)$ in Eq. (5) by effective coefficients $\tilde{v}_{k_1k_2q}(R)$. The latter are then determined by constraining the energies resulting from the diagonalization of $H_0+\tilde{V}$ to reproduce available adiabatic potential energies relevant to the $5\,^2P$ level of Rb. We believe that our previous pseudopotential molecular-structure calculations[21] which have been performed for the symmetry groups $C_{\infty v}$ and C_{2v} are sufficiently accurate for this purpose. Hereafter, we use the convention that the azimuthal angle of the H_2 internuclear axis is zero (defining the reference plane as Axz), γ specifying its orientation with respect to $\mathbf{R}$ (Az axis). Then, a convenient choice of the atomic basis set for diagonalizing $H_0+\tilde{V}$ is to consider the three state vectors $|p_k\rangle$ ($k\equiv x,y,z$) generating the $5\,^2P$ level of Rb, with corresponding electronic wave functions $\psi(p_k)$ defined as

$$\psi(p_x)=\frac{R(r_1)}{r_1}\frac{1}{\sqrt{2}}[Y_{1-1}(\hat{\mathbf{r}}_1)-Y_{11}(\hat{\mathbf{r}}_1)]\ , \tag{9a}$$

$$\psi(p_y)=\frac{iR(r_1)}{r_1}\frac{1}{\sqrt{2}}[Y_{1-1}(\hat{\mathbf{r}}_1)+Y_{11}(\hat{\mathbf{r}}_1)]\ , \tag{9b}$$

$$\psi(p_z)=\frac{R(r_1)}{r_1}Y_{10}(\hat{\mathbf{r}}_1)\ , \tag{9c}$$

where $R(r_1)$ is the radial wave function of the $5\,^2P$ level of Rb. Under a reflection with respect to the reference plane Axz, $|p_x\rangle$ and $|p_z\rangle$ are symmetrical and $|p_y\rangle$ is antisymmetrical. Then, $|p_x\rangle$ as well as $|p_z\rangle$ spans an irreducible representation A' of the symmetry group C_s, and $|p_y\rangle$ spans an irreducible representation A'' of the same group. Consequently, the nonzero matrix elements of $\tilde{V}(\mathbf{r}_1,R,\gamma\neq 0,\pi/2)$ are $\tilde{V}_{xx}$, $\tilde{V}_{yy}$, $\tilde{V}_{zz}$, and $\tilde{V}_{xz}=\tilde{V}_{zx}$, which can be written in terms of coefficients $\tilde{v}_{k_1k_2q}(R)$ from Eq. (2). Then, it is straightforward to find that the adiabatic potential energy surface of symmetry A'' associated with the $5\,^2P$ level of Rb is just $E_{A\,A''}(R,\gamma)=\tilde{V}_{yy}(R,\gamma)+\varepsilon_0$, where ε_0 is the energy of the $5\,^2P$ level; and the two adiabatic potential energy surfaces of symmetry A', noted $E_{B\,A'}(R,\gamma)$ and $E_{C\,A'}(R,\gamma)$, result from the diagonalization of the two-dimensional symmetrical matrix defined by $\tilde{V}_{xx}$, $\tilde{V}_{xz}$, and $\tilde{V}_{zz}$. Thus, the adiabatic potential energy surfaces relevant to the $5\,^2P$ level of Rb can be easily obtained from the knowledge of the coefficients $\tilde{v}_{k_1k_2q}(R)$. Similarly, it can be shown that (see Ref. 15, for example) the set $\{|p_x\rangle,|p_y\rangle\}$ spans an irreducible representation Π, and $|p_z\rangle$ spans an irreducible representation Σ of the symmetry group $C_{\infty v}$; and finally, $|p_x\rangle$, $|p_y\rangle$, and $|p_z\rangle$ span, respectively, the irreducible representation B_2, B_1, A_1 of the symmetry group C_{2v}. Therefore, $\tilde{V}(\mathbf{r}_1,R,\gamma=0,\pi/2)$ is diagonal in the basis set $\{|p_k\rangle\}$ and the adiabatic potential energy curves of the symmetry groups $C_{\infty v}$ and C_{2v} are immediately obtained:

$$E_{A\,\Pi}(R)=\tilde{V}_{xx}(R,0)+\varepsilon_0=\tilde{V}_{yy}(R,0)+\varepsilon_0\ ,$$

$$E_{B\,\Sigma}(R)=\tilde{V}_{zz}(R,0)+\varepsilon_0\ ,$$

$$E_{A\,B_2}(R)=\tilde{V}_{xx}\left[R,\frac{\pi}{2}\right]+\varepsilon_0\ ,$$

$$E_{A\,B_1}(R)=\tilde{V}_{yy}\left[R,\frac{\pi}{2}\right]+\varepsilon_0\ ,$$

and

$$E_{B\,A_1}(R)=\tilde{V}_{zz}\left[R,\frac{\pi}{2}\right]+\varepsilon_0\ .$$

For given R, constraining the adiabatic potential energies of the symmetries $C_{\infty v}$ and C_{2v} defined above to equal those previously calculated[21] leads one to define a set of five linear equations in $\tilde{v}_{k_1k_2q}(R)$. Generally, the number of coefficients $\tilde{v}_{k_1k_2q}(R)$ may be larger than five since k_2 can take even values up to 8 as mentioned above. Moreover, it is important to notice that q can only take the values 0,1,2 since $k_1=0,2$, and the coefficients $\tilde{v}_{k_1k_2q}(R)$ with $q=1$ cannot be involved for the symmetry groups $C_{\infty v}$ and C_{2v}. Therefore, as in Ref. 26, one finds that if $k_2=0,2$ only, the coefficients $\tilde{v}_{000}$, $\tilde{v}_{020}$, $\tilde{v}_{200}$, $\tilde{v}_{220}$, and $\tilde{v}_{222}$ can be uniquely obtained (the set of the five linear equations in $\tilde{v}_{k_1k_2q}(R)$ is identical to that of Ref. 26, except that k_1 and k_2 are exchanged and Ayz is chosen as reference plane). The only coefficient which cannot be determined from the symmetry groups $C_{\infty v}$ and C_{2v}, when limiting k_2 to take only the values 0 and 2, is $\tilde{v}_{221}(R)$. At this point, it is important to remark that the latter only defines the off-diagonal matrix element

$$\tilde{V}_{xz}(R,\gamma)=-\tilde{v}_{221}(R)P_2^1(\cos\gamma)\ . \tag{10}$$

Since the three-body interaction $V(\mathbf{r}_1,R,\gamma)$ is explicitly known from Ref. 21, the coefficient $\tilde{v}_{221}(R)$ has been determined directly from Eq. (2), that is, $\tilde{v}_{221}(R)=\bar{v}_{221}(R)$.

As already mentioned above, k_2 can take even values up to 8 in the present study. Therefore, it is impossible to determine uniquely all the coefficients $\tilde{v}_{k_1k_2q}(R)$ from only the symmetry groups $C_{\infty v}$ and C_{2v}. Then, our procedure has been as follows: the additional coefficients $\tilde{v}_{k_1k_2q}(R)$, with $k_2>2$, which are required in the expressions of the adiabatic potential energies for the symmetry groups $C_{\infty v}$ and C_{2v} are also determined from Eq. (2) and the explicit knowledge of $V(\mathbf{r}_1,R,\gamma)$. Then, the five coefficients above mentioned are obtained uniquely and consistently with the additional coefficients. The explicit expression of $V(\mathbf{r}_1,R,\gamma)$ in Ref. 21 allows one to determine the coefficients $\tilde{v}_{040}(R)$, $\tilde{v}_{060}(R)$, and $\tilde{v}_{080}(R)$, the other ones being zero. Taking into consideration these coefficients, which have significant values only for $R\lesssim 3$ a.u., modifies little the five coefficients determined when $k_2=0,2$ only; the latter have practically converged after the introduction of $\tilde{v}_{040}(R)$. Figure 1 shows the most

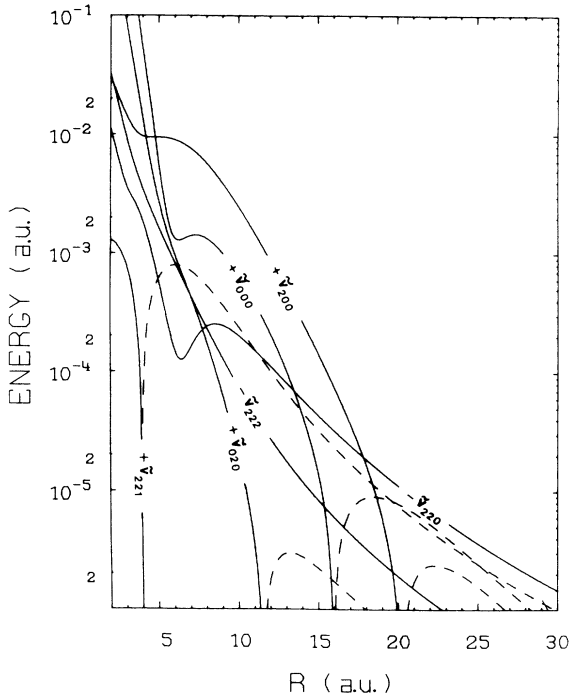

FIG. 1. Spherical harmonic expansion coefficients $\tilde{v}_{k_1k_2q}(R)$ (see Secs. II A and II B) as indicated in the figure. When a coefficient changes sign, its negative part is represented by a dashed line without ambiguity.

important coefficients $\tilde{v}_{k_1k_2q}(R)$ which have been determined by this procedure. In particular, it can be seen that $\tilde{v}_{221}(R)$ takes quite small values. In Ref. 26 this term has been neglected. However, its consideration is of prime importance for determining realistic potential energy surfaces, as shown in the following.

C. Adiabatic potential energy surfaces

Given the coefficients $\tilde{v}_{k_1k_2q}(R)$, the adiabatic potential energy surfaces associated with the $5\,^2P$ level of Rb can be easily obtained as indicated in the preceding section. Figure 2 shows, as an example, the adiabatic potential energy curves obtained for $\gamma=0°$, 60°, and 90°. The correlations of the adiabatic potential energy surfaces of the symmetry group C_s with the adiabatic potential energy curves of the symmetry groups $C_{\infty v}$ and C_{2v} are summarized as follows:

$$\sup\{E_{B\Sigma}(R),E_{A\Pi}(R)\}\leftarrow E_{CA'}(R,\gamma) \rightarrow \sup\{E_{BA_1}(R),E_{AB_2}(R)\}\ , \quad (11a)$$

$$E_{A\Pi}(R)\leftarrow E_{AA''}(R,\gamma)\rightarrow E_{AB_1}(R)\ , \quad (11b)$$

$$\inf\{E_{B\Sigma}(R),E_{A\Pi}(R)\}\leftarrow E_{BA'}(R,\gamma) \rightarrow \inf\{E_{BA_1}(R),E_{AB_2}(R)\}\ , \quad (11c)$$

where $\inf\{E_1,E_2\}$, $\sup\{E_1,E_2\}$ means, respectively, the lowest and the highest of the two energies E_1 and E_2.

It is important to notice that the potential surfaces

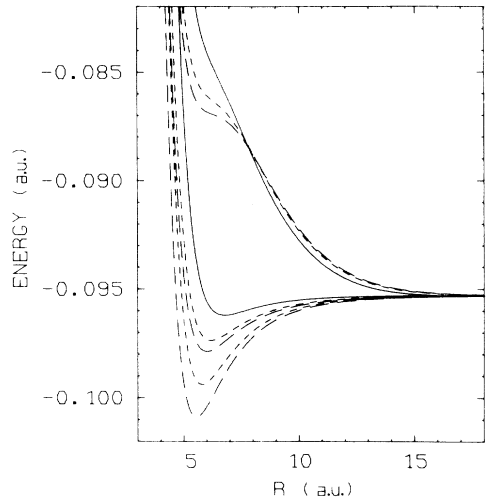

FIG. 2. Adiabatic potential energy curves for the Rb($5\,^2P$)-H_2 or D_2 system. Solid lines ($\gamma=0$), $E_{A\Pi}(R)<E_{B\Sigma}(R)$; short-dashed lines ($\gamma=60°$), $E_{BA'}(R,\gamma)<E_{AA''}(R,\gamma)<E_{CA'}(R,\gamma)$; long-dashed lines ($\gamma=90°$), $E_{AB_2}(R)<E_{AB_1}(R)<E_{BA_1}(R)$.

$E_{BA'}(R,\gamma)$ and $E_{CA'}(R,\gamma)$ cannot intersect since they are of same symmetry, but they are correlated with the potential curves $E_{A\Pi}(R)$ and $E_{B\Sigma}(R)$ which, from our previous calculations,[21] intersect at $R=R_0=16.13$ a.u. Therefore a conical intersection of the potential surface at R_0 for $\gamma=0°$ (Ref. 27) follows, which is illustrated in Fig. 3(a) by a three-dimensional representation of the surfaces near R_0.

As already mentioned above, $\tilde{v}_{221}(R)$ determines the off-diagonal matrix element $\tilde{V}_{xz}(R,\gamma)$ [see Eq. (10)]. If one takes $\tilde{v}_{221}(R)\equiv 0$, then $\tilde{V}(R,\gamma)$ is diagonal for any value of γ. In other words, the Hamiltonian of the system which is normally invariant under the symmetry group C_{2v} for the only value $\gamma=90°$ becomes invariant under C_{2v} for any value $\gamma\neq 0$. This has the following consequences. The adiabatic potential energy surfaces of the symmetry group C_s are replaced by unrealistic potential energy surfaces $\tilde{E}_{BA_1}(R,\gamma)$ and $\tilde{E}_{AB_2}(R,\gamma)$ of the symmetry group C_{2v} which can now intersect along a curve as illustrated in Fig. 3(b), and $\tilde{E}_{AB_1}(R,\gamma)\equiv E_{AA''}(R,\gamma)$. Moreover, it can be shown[15] that the intersection of the curves $\tilde{E}_{BA_1}(R_0,\gamma)$ and $\tilde{E}_{AB_2}(R_0,\gamma)$ is tangential rather than conical for $\gamma=0°$.

A detailed study of the symmetries of the system when the spin-orbit interaction in Rb is considered may be found in Ref. 15. The results are summarized as follows.

One considers a spin-orbit interaction which is taken to be independent of r_1,

$$V_{SO}=A\,\mathbf{L}_1\cdot\mathbf{S}_1\ , \quad (12)$$

where $\mathbf{L}_1$ and $\mathbf{S}_1$ are, respectively, the orbital angular momentum and the spin momentum of e^-. In the case of the $5\,^2P$ level of Rb, $A=\frac{2}{3}\Delta\varepsilon$ with $\Delta\varepsilon$ the energy splitting of the $5\,^2P_{1/2}$ and $5\,^2P_{3/2}$ levels ($\Delta\varepsilon=1.08\times10^{-3}$ a.u.$=237.6$ cm^{-1}). In order to diagonalize the full Hamiltonian $H=H_0+\tilde{V}+V_{SO}$, it is now convenient

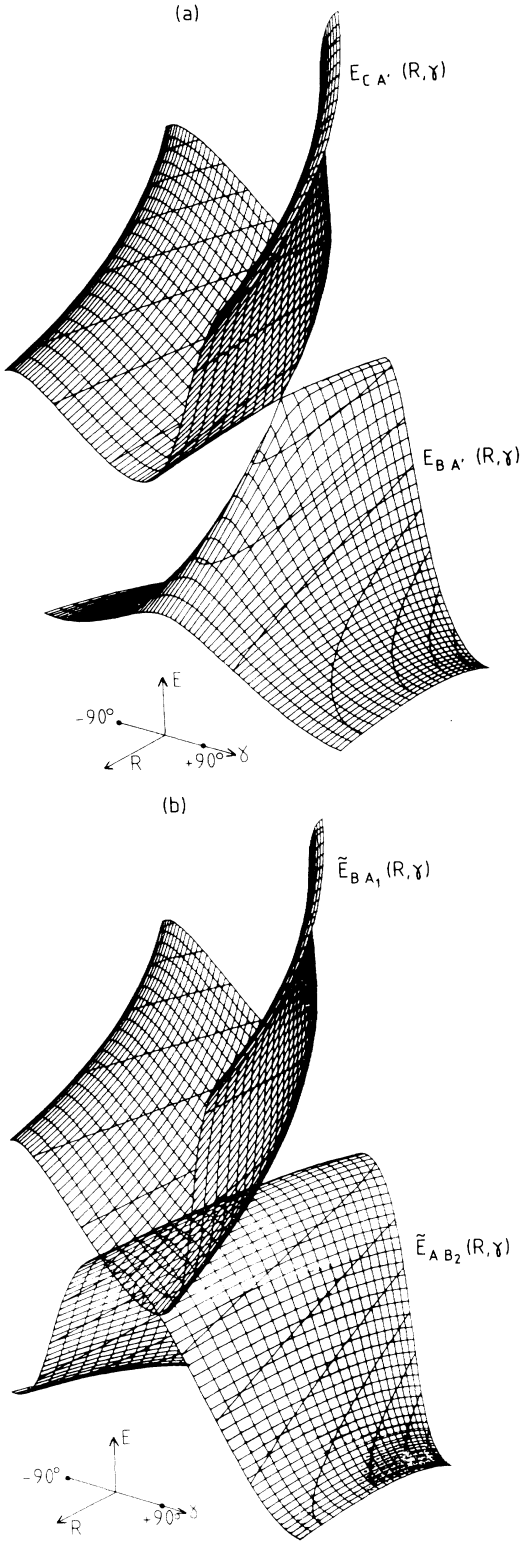

FIG. 3. (a) Adiabatic potential energy surfaces $E_{BA'}(R,\gamma)$ and $E_{CA'}(R,\gamma)$ in the conical intersection region $R_0 \simeq 16.1$ a.u. γ varies between $-90°$ and $+90°$ and R between 15.1 and 17.1 a.u. (b) Unrealistic adiabatic potential energy surfaces $\tilde{E}_{AB_2}(R,\gamma)$ and $\tilde{E}_{BA_1}(R,\gamma)$ (see Sec. II C) in the region $R_0 \simeq 16.1$ a.u., as in (a).

to use an atomic basis set generating the $5\,^2P_{j_1}$ levels of Rb in which H_0 and V_{SO} are diagonal. After a particular unitary transformation, the six state vectors $|j_1 m_1\rangle$ which are eigenvectors of J_1^2 and J_{1z} ($\mathbf{J}_1=\mathbf{L}_1+\mathbf{S}_1$) lead to three sets of two state vectors:

$$|\tfrac{1}{2}\tfrac{1}{2}\rangle^{\nu} \equiv \frac{1}{\sqrt{2}}\{|\tfrac{1}{2}\tfrac{1}{2}\rangle + i\nu|\tfrac{1}{2}-\tfrac{1}{2}\rangle\}\ , \tag{13a}$$

$$|\tfrac{3}{2}\tfrac{1}{2}\rangle^{-\nu} \equiv \frac{1}{\sqrt{2}}\{|\tfrac{3}{2}\tfrac{1}{2}\rangle - i\nu|\tfrac{3}{2}-\tfrac{1}{2}\rangle\}\ , \tag{13b}$$

$$|\tfrac{3}{2}\tfrac{3}{2}\rangle^{-\nu} \equiv \frac{1}{\sqrt{2}}\{|\tfrac{3}{2}\tfrac{3}{2}\rangle + i\nu|\tfrac{3}{2}-\tfrac{3}{2}\rangle\}\ , \tag{13c}$$

with $\nu=\pm 1$. Since one considers half-integer spin state vectors, the set of state vectors $\{|\frac{1}{2}\frac{1}{2}\rangle^{+1}, |\frac{1}{2}\frac{1}{2}\rangle^{-1}\}$ as well as the set $\{|\frac{3}{2}\frac{1}{2}\rangle^{-1}, |\frac{3}{2}\frac{1}{2}\rangle^{+1}\}$ spans the same half-integer irreducible representation of the symmetry group $C_{\infty v}$; this two-dimensional irreducible representation, labeled by the absolute value $|m_1|=\frac{1}{2}$, is noted 1/2. Moreover, the set $\{|\frac{3}{2}\frac{3}{2}\rangle^{-1}, |\frac{3}{2}\frac{3}{2}\rangle^{+1}\}$ spans the half-integer two-dimensional irreducible representation of the symmetry group $C_{\infty v}$, labeled by $|m_1|=\frac{3}{2}$ and noted 3/2. If now the symmetry group C_{2v} or C_s is considered, each of the three set of state vectors defined by Eqs. (13a)–(13c) spans the same two-dimensional irreducible representation, noted 1/2. Then, one comes to the result that, in all events, the eigenvalues of H are doubly degenerate and the six-dimensional matrix (H_{ij}) defined by the state vectors (13a)–(13c) is block diagonal for each value of ν and each irreducible representation. Therefore, we have arbitrarily chosen $\nu=+1$. For convenience, we will use the notation $|1\rangle \equiv |\frac{1}{2}\frac{1}{2}\rangle^{+}$, $|2\rangle \equiv |\frac{3}{2}\frac{1}{2}\rangle^{-}$, $|3\rangle \equiv |\frac{3}{2}\frac{3}{2}\rangle^{-}$. Now, because the electronic part of the wave functions associated with the state vectors $|i\rangle$ are related to the functions $\psi(p_k)$ defined by Eqs. (9a)–(9c) the matrix elements of $\tilde{V}(\mathbf{r}_1,R,\gamma)$ can be written in terms of matrix elements $\tilde{V}_{xx}$, $\tilde{V}_{yy}$, $\tilde{V}_{zz}$, and $\tilde{V}_{xz}$ previously obtained. The Hermitian matrix (H_{ij}) is then defined by

$$H_{11} = \tfrac{1}{3}(\tilde{V}_{xx}+\tilde{V}_{yy}+\tilde{V}_{zz}) + \varepsilon_0 - \tfrac{2}{3}\Delta\varepsilon\ , \tag{14a}$$

$$H_{12} = \frac{\sqrt{2}}{6}(\tilde{V}_{xx}+\tilde{V}_{yy}) - \frac{\sqrt{2}}{3}\tilde{V}_{zz} + \frac{i}{\sqrt{2}}\tilde{V}_{xz}\ , \tag{14b}$$

$$H_{13} = \frac{1}{\sqrt{6}}\tilde{V}_{xz} - \frac{i}{\sqrt{2}}(\tilde{V}_{xx}-\tilde{V}_{yy})\ , \tag{14c}$$

$$H_{22} = \tfrac{1}{6}(\tilde{V}_{xx}+\tilde{V}_{yy}) + \tfrac{2}{3}\tilde{V}_{zz} + \varepsilon_0 + \tfrac{1}{3}\Delta\varepsilon\ , \tag{14d}$$

$$H_{23} = -\frac{1}{\sqrt{3}}\tilde{V}_{xz} - \frac{i}{\sqrt{2}}(\tilde{V}_{xx}-\tilde{V}_{yy})\ , \tag{14e}$$

$$H_{33} = \tfrac{1}{2}(\tilde{V}_{xx}+\tilde{V}_{yy}) + \varepsilon_0 + \tfrac{1}{3}\Delta\varepsilon\ . \tag{14f}$$

One may verify immediately that the adiabatic potential energy associated with the irreducible representation 3/2 of the symmetry group $C_{\infty v}$ is just $E_{A\,3/2}(R) = H_{33}(R,0) = E_{A\Pi}(R) + \varepsilon_0 + \frac{1}{2}\Delta\varepsilon$. The adiabatic potential energies associated with the irreducible representation 1/2 of $C_{\infty v}$ result from the diagonalization of a two-dimensional matrix, and are noted $E_{B\,1/2}(R)$ and

$E_{C\,1/2}(R)$ (note that $E_{B\,1/2}(R)$ is correlated with the $5\,^2P_{1/2}$ level, while $E_{C\,1/2}(R)$ is correlated with the $5\,^2P_{3/2}$ level). From Eqs. (14a)–(14f) it can be verified that the adiabatic potential energies of the representations 1/2 of the symmetry groups C_{2v} and C_s result from the diagonalization of a three-dimensional matrix (H_{ij}); they are noted $E_{B\,1/2}(R,\gamma)$, $E_{C\,1/2}(R,\gamma)$, and $E_{D\,1/2}(R,\gamma)$. The correlations of the latter with the potential energy curves of the symmetry group $C_{\infty v}$ may be summarized as follows:

$$\sup\{E_{C\,1/2}(R),E_{A\,3/2}(R)\}\leftarrow E_{D\,1/2}(R,\gamma)\ , \tag{15a}$$

$$\inf\{E_{C\,1/2}(R),E_{A\,3/2}(R)\}\leftarrow E_{C\,1/2}(R,\gamma)\ , \tag{15b}$$

$$E_{B\,1/2}(R)\leftarrow E_{B\,1/2}(R,\gamma)\ . \tag{15c}$$

Figure 4 shows, as an example, the adiabatic potential energy curves obtained for $\gamma=0°$, 60°, and 90°. It can be shown that the potential curves $E_{A\,3/2}(R)$ and $E_{C\,1/2}(R)$ intersect at the same distance $R=R_0$ as do the potential curves $E_{A\Pi}(R)$ and $E_{B\Sigma}(R)$. Therefore, the potential surfaces $E_{C\,1/2}(R,\gamma)$ and $E_{D\,1/2}(R,\gamma)$ will exhibit a conical intersection at $R=R_0$, for $\gamma=0$, as illustrated in Fig. 5(a).

As before, one takes $\tilde{v}_{221}(R)\equiv 0$ and looks at the changes in the adiabatic potential energy surfaces. In that case, the Hamiltonian becomes again invariant under the symmetry group C_{2v} for any value $\gamma\neq 0$. The unrealistic adiabatic potential energy surfaces $\tilde{E}_{C\,1/2}(R,\gamma)$ and $\tilde{E}_{D\,1/2}(R,\gamma)$ which result from its diagonalization show a tangential intersection at $R=R_0$, for $\gamma=0$, as do the corresponding unrealistic potential energy surfaces $\tilde{E}_{BA_1}(R,\gamma)$ and $\tilde{E}_{AB_2}(R,\gamma)$ obtained when the spin-orbit interaction is ignored. However, the potential surfaces $\tilde{E}_{C\,1/2}(R,\gamma)$ and $\tilde{E}_{D\,1/2}(R,\gamma)$, which are of same symmetry, cannot intersect for $\gamma\neq 0$. Therefore, the intersection of the corresponding unrealistic potential surfaces $\tilde{E}_{BA_1}(R,\gamma)$ and $\tilde{E}_{AB_2}(R,\gamma)$ along a line [see Fig. 3(b)] is changed by the spin-orbit interaction into an avoided crossing of the unrealistic potential surfaces $\tilde{E}_{C\,1/2}(R,\gamma)$ and $\tilde{E}_{D\,1/2}(R,\gamma)$, as clearly seen in Fig. 5(b).

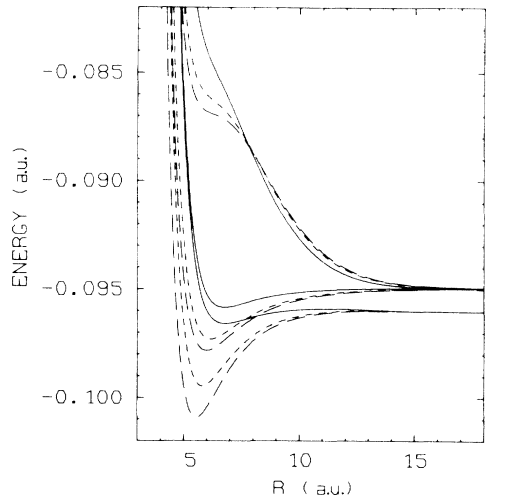

FIG. 4. Adiabatic potential energy curves for the Rb-H_2 or D_2 system correlated with the $5\,^2P_{1/2}$ and $5\,^2P_{3/2}$ levels of Rb. Solid lines ($\gamma=0$), $E_{B\,1/2}(R)<E_{A\,3/2}(R)<E_{C\,1/2}(R)$; short-dashed lines ($\gamma=60°$) and long-dashed lines ($\gamma=90°$), $E_{B\,1/2}(R,\gamma)<E_{C\,1/2}(R,\gamma)<E_{D\,1/2}(R,\gamma)$.

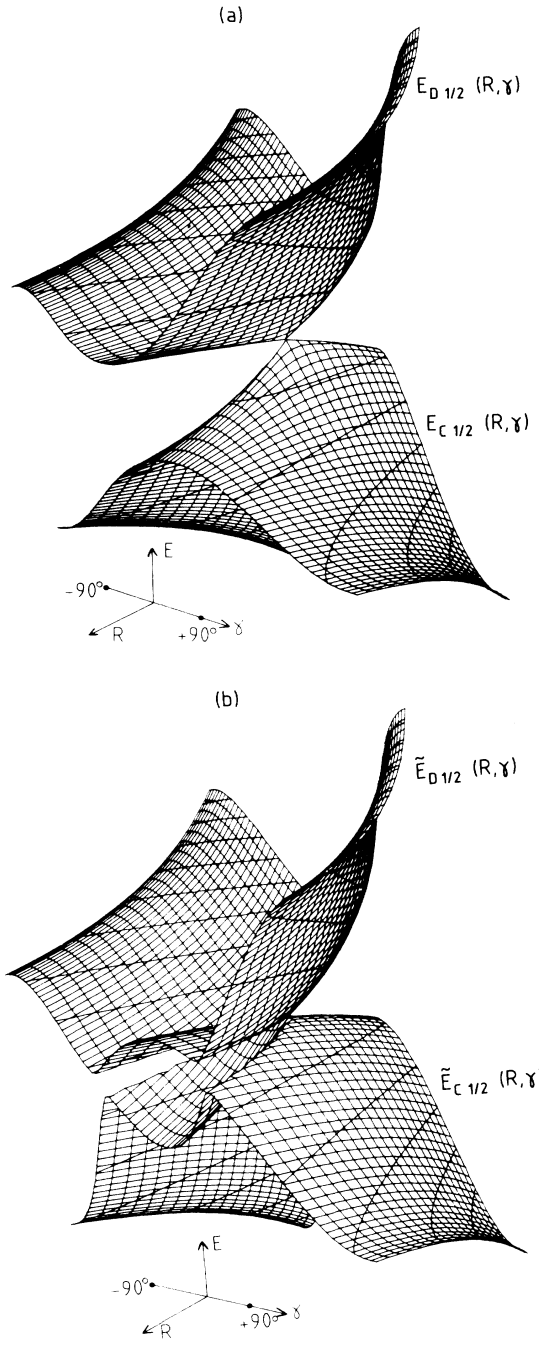

FIG. 5. (a) Adiabatic potential energy surfaces $E_{C\,1/2}(R,\gamma)$ and $E_{D\,1/2}(R,\gamma)$ in the region $R_0\simeq 16.1$ a.u., as in Fig. 3(a). (b) Unrealistic potential energy surfaces $\tilde{E}_{C\,1/2}(R,\gamma)$ and $\tilde{E}_{D\,1/2}(R,\gamma)$ (see Sec. II C) in the region $R_0\simeq 16.1$ a.u., as in Fig. 3(a).

In conclusion of this section, one may assert that the coefficient $\bar{v}_{221}(R)$ is very important, in spite of its smallness, for determining realistic adiabatic potential energy surfaces.

D. Evaluation of nonadiabatic coupling matrix elements

Since the internuclear distance r_2 of M is kept constant during the collision (rigid-rotor approximation), the only nonadiabatic coupling components which may be considered are (see Refs. 4 and 28, for example) a radial component with matrix elements

$$d_{ij}^{(R)}(R,\gamma)=\left\langle \psi_i \left| \frac{\partial}{\partial R} \right| \psi_j \right\rangle \tag{16}$$

and an angular component, with matrix elements

$$d_{ij}^{(\gamma)}(R,\gamma)=\frac{1}{R}\left\langle \psi_i \left| \frac{\partial}{\partial \gamma} \right| \psi_j \right\rangle . \tag{17}$$

The Coriolis coupling which results from the rotation of the internuclear axis **R** during the collision is not considered in this paper. In Eqs. (16) and (17) the molecular wave functions ψ_k (with $k \equiv 1,2,3$) correspond to the three adiabatic potential energy surfaces ordered according to increasing energies and correlating with the $5\,^2P_{1/2}$ and $5\,^2P_{3/2}$ levels of Rb. They can be easily derived from the diagonalization of the matrix (H_{ij}) defined by Eqs. (14a)–(14f). One may write

$$\psi_k = \sum_i a_i^k(R,\gamma)\varphi_i(\mathbf{r},\sigma) , \tag{18}$$

where the wave functions φ_i are associated with the three state vectors defined by Eqs. (13a)–(13c), σ denoting the spin variable. Then, the nonadiabatic coupling matrix elements $d_{ij}^{(x)}(R,\gamma)$, with $x \equiv R$ or γ, can be easily evaluated from numerical derivative of the coefficients $a_i^k(R,\gamma)$. As already discussed elsewhere,[29] one verifies that

$$d_{ij}^{(x)}(R,\gamma)=-(d_{ji}^{(x)}(R,\gamma))^* \tag{19}$$

and the real parts of the diagonal terms are zero. One verifies also that in the case of the symmetry groups $C_{\infty v}$ and C_{2v}, or when one takes $v_{221}(R)\equiv 0$, the coupling matrix elements are real. All the nonadiabatic coupling matrix elements $d_{ij}^{(x)}(R,\gamma)$ among the three molecular wave functions ψ_k have been evaluated as described above. However, we concentrate in this paper on the off-diagonal coupling matrix elements, and more particularly on those taking significant values.

First, we consider the radial component of the nonadiabatic coupling. The radial coupling matrix elements $d_{12}^{(R)}$ and $d_{13}^{(R)}$ are particularly interesting since they are directly related to fine-structure transitions. Figure 6 shows the modulus of $d_{13}^{(R)}(R,\gamma)$ for different orientations γ of M. This coupling is characterized by a broad maximum near $R \simeq 12$ a.u., which changes little with γ. As discussed by Nikitin for $A(n\,^2P)$ + rare-gas collisions,[16] the maximum in radial coupling $d_{13}^{(R)}(R,0)$ is related to the spin-orbit decoupling occurring when the modulus of the difference between the potential curves

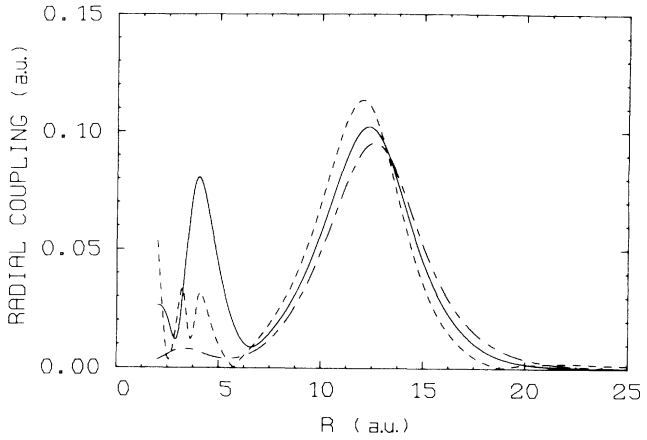

FIG. 6. Radial coupling matrix element $d_{13}^{(R)}(R,\gamma)$ vs R for $\gamma=0°$ (short-dashed line), $\gamma=45°$ (solid line), and $\gamma=90°$ (long-short-dashed line).

$E_{A\Pi}(R)$ and $E_{B\Sigma}(R)$ equals the spin-orbit splitting $\Delta\varepsilon$. For given $\gamma\neq 0$, this maximum may also be attributed to the spin-orbit decoupling occurring when the modulus of the difference between the $E_{BA_1}(R,\pi/2)$ and $E_{AB_2}(R,\pi/2)$ or $E_{CA'}(R,\gamma)$ and $E_{BA'}(R,\gamma)$ potential curves equals $\Delta\varepsilon$. In particular, the slight shift of the position of this maximum towards larger R values for $\gamma=90°$ may be easily understood from Fig. 2. At shorter R, $d_{13}^{(R)}(R,\gamma)$ exhibits a structure which changes much with γ, and which results from mixing of electronic molecular states. In particular, $d_{13}^{(R)}(R,\gamma)$ may show a relatively broad maximum at short distances, with an amplitude comparable with that of the outermost maximum previously discussed (see Fig. 6, for $\gamma=45°$). However, because this structure occurs in an R region where the potential energy curves are strongly repulsive (see Fig. 2), it should contribute significantly to the collisional processes only for relatively large collision energies. It is worthwhile to note also the similarity of the $d_{13}^{(R)}(R,0)$ radial coupling with that which has been ob-

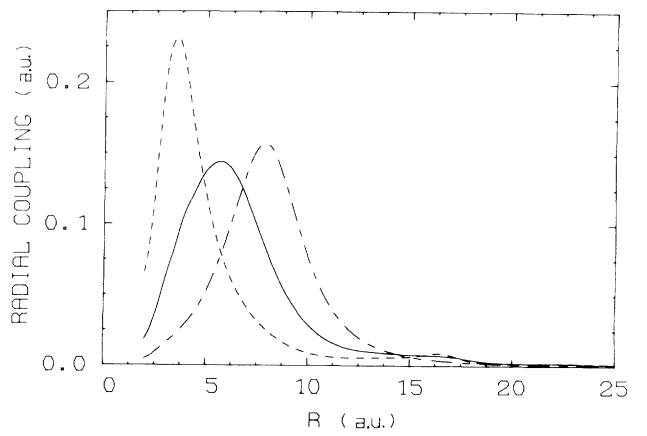

FIG. 7. Radial coupling matrix element $d_{12}^{(R)}(R,\gamma)$ vs R for $\gamma=15°$ (short-dashed line), $\gamma=30°$ (solid line), and $\gamma=90°$ (long-short-dashed line).

tained for Rb($5\,^2P$) + He collisions.[30] When taking $\tilde{v}_{221}(R)\equiv 0$ the outermost maximum of the coupling is little affected, while the structure at short internuclear distance for $\gamma\neq 0$, 90°, becomes comparable with that observed for $\gamma=90°$.

Figure 7 shows the modulus of the radial coupling $d_{12}^{(R)}(R,\gamma)$ for different values of γ. It is mainly characterized by a large maximum at short internuclear distances ($R\lesssim 8$ a.u.). For $\gamma\gtrsim 30°$ one finds that this maximum is broad; its position shifts towards larger values of R for $\gamma\rightarrow 90°$, but its amplitude does not change much. For $\gamma\rightarrow 0°$, the coupling term becomes very sharp, the amplitude of its maximum increasing drastically. As discussed by Hickman,[13,14] the maximum in $d_{12}^{(R)}(R,\gamma\neq 0)$ may also be attributed to a spin-orbit decoupling occurring when the difference between the $E_{AB_1}(R)$ and $E_{AB_2}(R)$ potential curves or $E_{AA''}(R,\gamma)$ and $E_{BA'}(R,\gamma)$ potential surfaces equals $\Delta\varepsilon$. Moreover, because the potential surfaces $E_{AA''}(R,\gamma)$ and $E_{BA'}(R,\gamma)$ merge into the potential curve $E_{A\Pi}(R)$ for $\gamma=0°$, the coupling term becomes infinite for $\gamma=0°$. It is important to notice that the maximum in radial coupling $d_{12}^{(R)}(R,\gamma)$ occurs for distances R where the potential curves are attractive (see Fig. 2). Therefore, $d_{12}^{(R)}(R,\gamma)$ should be quite important for inducing fine-structure transitions, in agreement with the conclusions of Hickman.[13] When taking $\tilde{v}_{221}(R)\equiv 0$, only slight changes are observed in radial coupling $d_{12}^{(R)}(R,\gamma)$.

Figure 8 shows the modulus of the radial coupling $d_{23}^{(R)}(R,\gamma)$ for different values of γ. It is mainly characterized by a large maximum at intermediate distances ($R\simeq 16$–21 a.u.) which changes much with γ. For $\gamma=90°$, the maximum in the coupling term is very broad and its amplitude is the smallest. For γ decreasing from 90° to 0°, the maximum becomes better and better located; its amplitude increases rapidly and its position shifts towards shorter distances R, with the limit $R\simeq 16$ a.u. for $\gamma\rightarrow 0°$. This maximum is clearly associated with the conical intersection of the potential surfaces at $R_0=16.1$ a.u., for $\gamma=0°$. As discussed in Sec. II C, large changes in the potential surfaces are observed near the conical intersection when taking $\tilde{v}_{221}(R)\equiv 0$. Therefore, large changes in radial coupling $d_{23}^{(R)}(R,\gamma)$ should be also observed in that R region. Figures 9(a)–9(b) show comparatively, for $\gamma=30°$, the changes in the adiabatic po-

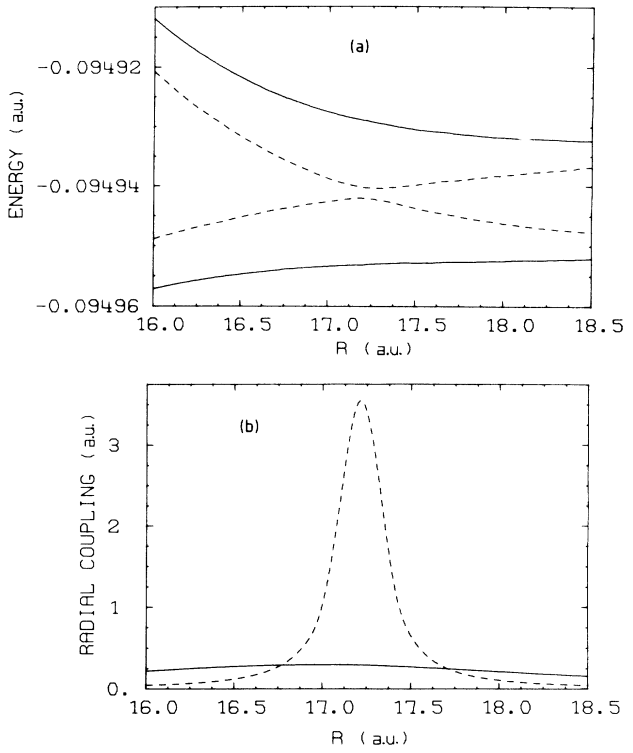

FIG. 9. (a) Adiabatic potential energy curves $E_{C\,1/2}(R,30°)$ and $E_{D\,1/2}(R,30°)$ (solid lines) and unrealistic potential curves $\tilde{E}_{C\,1/2}(R,30°)$ and $\tilde{E}_{D\,1/2}(R,30°)$ (dashed line, see Sec. II C) near the region of the conical intersection $R_0\simeq 16.1$ a.u. (b) Radial coupling matrix elements $d_{23}^{(R)}(R,\gamma)$ corresponding to the realistic (solid line) or unrealistic (dashed line) adiabatic potential curves of (a).

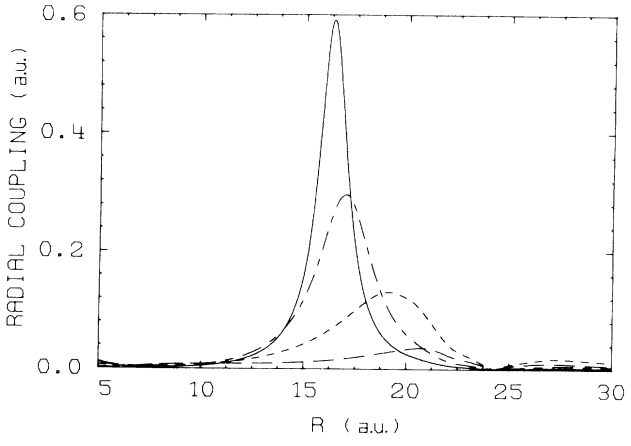

FIG. 8. Radial coupling matrix element $d_{23}^{(R)}(R,\gamma)$ vs R for $\gamma=15°$ (solid line), $\gamma=30°$ (long-short-dashed line), $\gamma=60°$ (short-dashed line), and $\gamma=90°$ (long-dashed line).

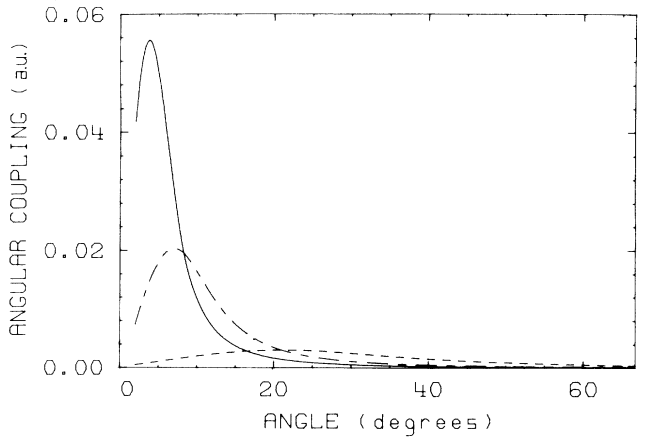

FIG. 10. Angular coupling matrix element $d_{12}^{(\gamma)}(R,\gamma)$ vs γ for $R=2$ a.u. (solid line), $R=3$ a.u. (long-short-dashed line), and $R=6$ a.u. (short-dashed line).

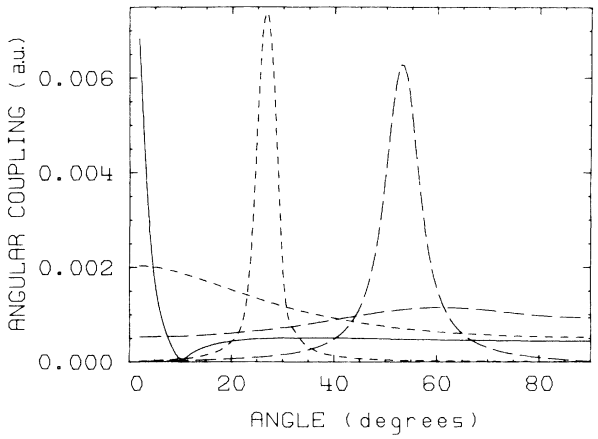

FIG. 11. Angular coupling matrix element $d_{23}^{(\gamma)}(R,\gamma)$ vs γ for $R=16$ a.u. (solid line), $R=17$ a.u. (short-dashed line), and $R=20$ a.u. (long-dashed line). In the case of $R=17$ and 20 a.u. two curves each are shown and the sharply peaked curves correspond to the unrealistic approximation with $\tilde{v}_{221}(R)\equiv 0$ (see text).

tential energy curves and in the radial coupling $d_{23}^{(R)}(R,\gamma)$ when taking $\tilde{v}_{221}(R)\equiv 0$ or not. For $\tilde{v}_{221}(R)\not\equiv 0$, there is no obvious crossing of the potential curves and the coupling term is rather flat. It should be noticed, however, that for $\gamma \lesssim 20°$ the potential curves present an avoided crossing near R_0, and in that case the coupling term becomes well located (see Fig. 8). When taking $\tilde{v}_{221}(R)\equiv 0$, the potential curves present an avoided crossing, which becomes more pronounced when γ goes to 0°, resulting in a well-located coupling term. As seen from Figs. 6–8, the radial coupling $d_{23}^{(R)}(R,\gamma)$ has an amplitude equal to or a larger than that of the radial coupling $d_{12}^{(R)}(R,\gamma)$ or $d_{13}^{(R)}(R,\gamma)$; but, since it corresponds to very small splitting between the potential curves [see Fig. 9(a)], the radial coupling $d_{23}^{(R)}(R,\gamma)$ is not expected to contribute significantly to the ${}^2P_{1/2}\rightarrow{}^2P_{3/2}$ transition, except perhaps near threshold of the transition or when polarization effects are studied for the reverse process.

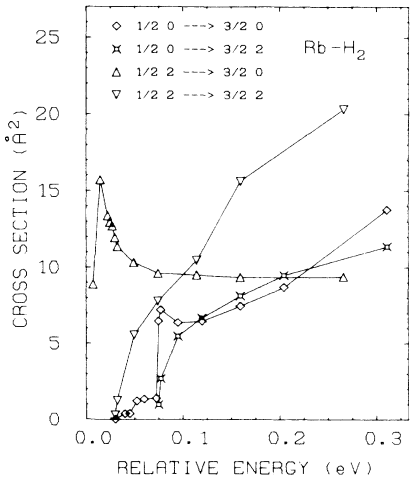

FIG. 12. Total cross sections for the $\frac{1}{2}j_2\rightarrow\frac{3}{2}j_2'$ transitions in Rb($5\,{}^2P$) + para-H_2 collisions vs the relative collision energy referring to the initial channel, for rotational levels 0 and 2, as indicated in the figure. The solid lines between the calculated points (symbols) have been drawn for guiding the eyes.

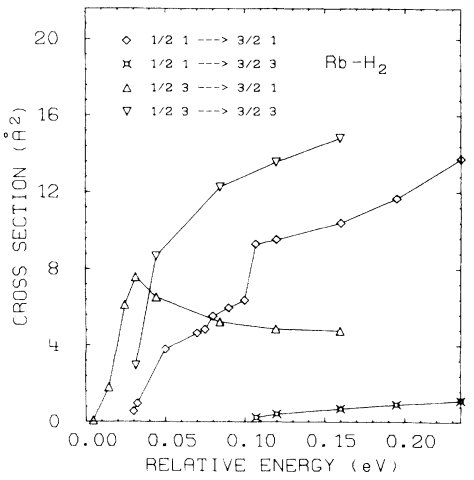

FIG. 13. Total cross sections for the $\frac{1}{2}j_2\rightarrow\frac{3}{2}j_2'$ transitions in Rb($5\,{}^2P$)+ortho-H_2 collisions, for rotational levels 1 and 3, as in Fig. 12.

We now consider the matrix elements $d_{ij}^{(\gamma)}(R,\gamma)$ of the angular component of the nonadiabatic coupling. They are found to be much smaller than the radial coupling $d_{ij}^{(R)}(R,\gamma)$. Figure 10 shows the modulus of the angular coupling $d_{12}^{(\gamma)}(R,\gamma)$ which is found to be sharply pointed at small values of both R and γ. As R increases, the maximum in the coupling term becomes broader; its position is shifted towards larger values of γ, and its amplitude decreases rapidly. Comparatively, the angular coupling terms $d_{13}^{(\gamma)}(R,\gamma)$ and $d_{23}^{(\gamma)}(R,\gamma)$ present the same features as $d_{12}^{(\gamma)}(R,\gamma)$ in the same region of R and γ, but

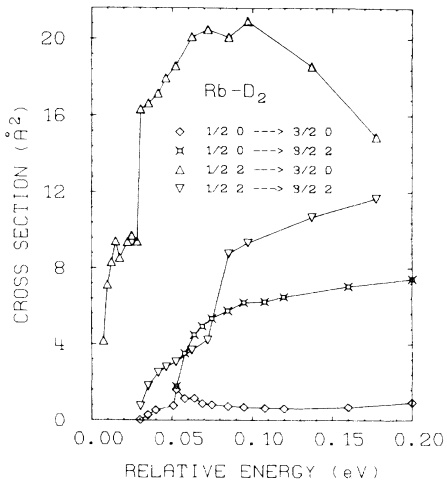

FIG. 14. Total cross sections for the $\frac{1}{2}j_2\rightarrow\frac{3}{2}j_2'$ transitions in Rb($5\,{}^2P$)+ortho-D_2 collisions, as in Fig. 12.

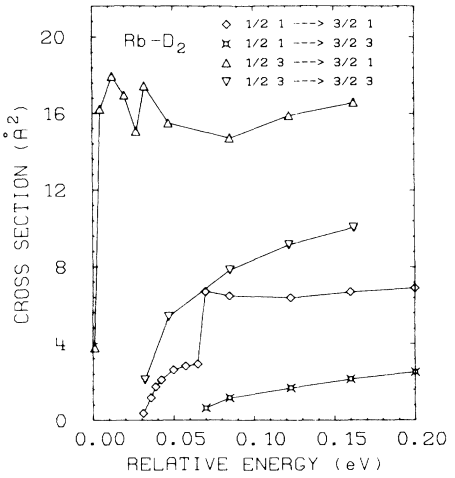

FIG. 15. Total cross sections for the $\frac{1}{2}j_2 \rightarrow \frac{3}{2}j_2'$ transitions in Rb($5\,^2P$)+para-D_2 collisions, as in Fig. 12.

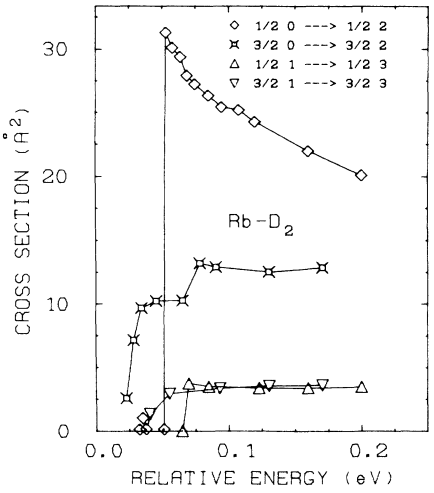

FIG. 17. Total cross sections for the $j_1 j_2 \rightarrow j_1 j_2'$ inelastic rotational transition in Rb($5\,^2P$)+ortho- or para-D_2, as in Fig. 16.

their amplitudes are much smaller by one or two orders of magnitude. However, it is interesting to note that the angular coupling $d_{23}^{(\gamma)}(R,\gamma)$ is sharply pointed at small values of γ in the region of the conical intersection R_0, and changes considerably when going through this region, as seen in Fig. 11 for $R=16$, 17, and 20 a.u. When taking $\tilde{v}_{221}(R)\equiv 0$, the changes in the angular coupling terms $d_{12}^{(\gamma)}(R,\gamma)$ and $d_{13}^{(\gamma)}(R,\gamma)$ are insignificant. But, as expected, the changes are considerable in angular coupling $d_{23}^{(\gamma)}(R,\gamma)$, as seen in Fig. 11 for $R=17$ and 20 a.u. One finds that for $R=16$ a.u., the peak in $d_{23}^{(\gamma)}(R,\gamma)$ disappears for small values of γ; for $R>R_0$, the coupling term becomes well located in the γ region where the unrealistic adiabatic potential energy surfaces present an avoided crossing [see Fig. 5(b)].

III. RESULTS AND DISCUSSION

The close-coupling calculations were carried out for relative collision energies E referring to the $|\frac{1}{2}0\rangle$ or $|\frac{1}{2}1\rangle$ channel from $\Delta\varepsilon=0.029$ eV (the fine-structure energy splitting of the $5\,^2P$ level of Rb) up to about 0.2–0.3 eV. Summations over the partial waves l, in Eq. (6), were made from $l=0$ up to a value $l_{\max}$ (depending upon the energy and the collisional system) where all the cross sections for the inelastic processes (1) have converged. For example, $l_{\max}\simeq 120$ for Rb($5\,^2P$)+para-H_2 collisions at a relative energy of 0.205 eV referring to the $|\frac{1}{2}0\rangle$ channel.

The calculated total cross sections for the fine-structure transitions in Rb with or without inelastic rotational transitions in M, that is, the $\frac{1}{2}j_2 \rightarrow \frac{3}{2}j_2'$ transitions, are reported in Figs. 12 and 13 for para- and ortho-H_2, and in Figs. 14 and 15 for ortho- and para-D_2 versus the collision energy E_R relative to the entrance channel $|\frac{1}{2}j_2\rangle$. For clarity of the figures, the cross sections for transitions involving the rotational levels j_2 or

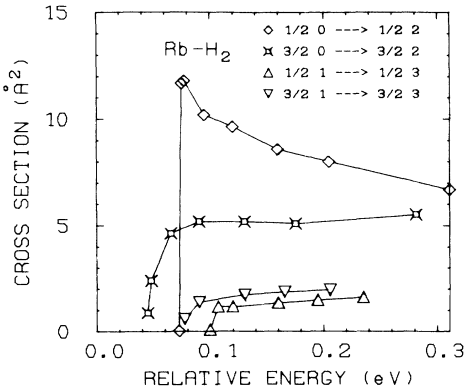

FIG. 16. Total cross sections for the $j_1 j_2 \rightarrow j_1 j_2'$ rotational transitions in Rb($5\,^2P$)+para- or ortho-H_2, for $j_1=\frac{1}{2}$ or $\frac{3}{2}$ and $j_2, j_2' \neq j_2$ taking the values 0,2 or 1,3 (as indicated in the figure).

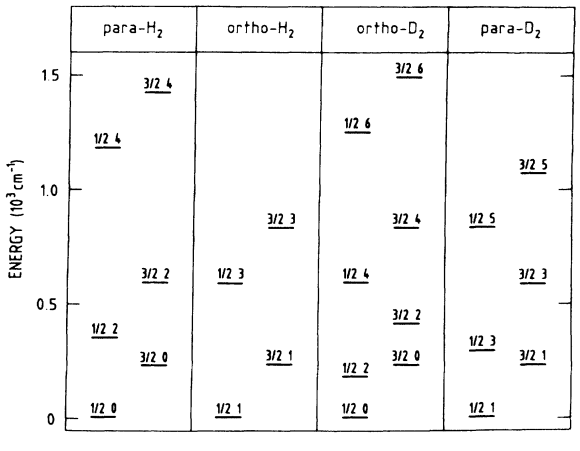

FIG. 18. Energy level diagrams for the four Rb($5\,^2P_{j_1}$)+para- or ortho-$M(j_2)$ systems, with $M\equiv H_2, D_2$. The energies of the levels are relative to the energy of the $\frac{1}{2}0$ or $\frac{1}{2}1$ level.

$j_2'=4$ are reported separately in Tables I and II. Note that the total cross sections for the $\frac{3}{2}j_2' \rightarrow \frac{1}{2}j_2$ reverse transitions can be obtained by the detailed balance. Similarly, the calculated total cross sections for $j_1j_2 \rightarrow j_1j_2'$ transitions, corresponding to inelastic rotational transitions $j_2 \rightarrow j_2'$ in M without fine-structure transitions in Rb, are reported in Fig. 16 for para- and ortho-H_2, and in Fig. 17 for ortho- and para-D_2; those involving j_2 or $j_2'=4$ are reported in Tables III and IV. For facilitating the discussion of these results, the energy level diagrams of the four Rb($5\,^2P_{j_1}$)-$M(j_2)$ systems are shown together in Fig. 18 where the rotational constant has been taken equal to 59.33 cm^{-1} for H_2 and to 29.91 cm^{-1} for D_2.[31]

The sudden variations of some cross sections with E_R which may be observed in Figs. 12–17 and Tables I–IV can be related to the opening of a new electronic rotational channel (see Fig. 18). Indeed, the effect (sudden enhancement or lowering of the cross sections) is seen to be more pronounced for the $j_1j_2 \rightarrow j_1'j_2'$ transitions when the opening rotational channel corresponds to the value $\min(j_2,j_2')+\Delta j_2$, with $\Delta j_2=2$, and when it is associated with the electronic channel $j_1'=\frac{3}{2}$. The effect is also visible for $\Delta j_2=4$, in the case of ortho-D_2. Thus, the effect seems to be closely related to the rotational energy splitting. As seen in Figs. 16 and 17 and Tables III and IV, the cross sections for rotational excitation of M are decreasing functions of the rotational energy splitting. In particular, these cross sections are comparatively larger for even than for odd values of j_2. Moreover, the cross section for the $\frac{1}{2}0 \rightarrow \frac{1}{2}2$ rotational transition takes the largest values, and behaves quite differently than that for the $\frac{3}{2}0 \rightarrow \frac{3}{2}2$ rotational transition, in contrast with any of the other rotational transition cross sections. The latter behave similarly, going rapidly and separately to a same constant value for $j_1=\frac{1}{2}$ or $\frac{3}{2}$, as the energy increases. The cross section for the $\frac{1}{2}0 \rightarrow \frac{1}{2}2$ transition is seen to increase drastically when the $|\frac{3}{2}2\rangle$ channel opens, and then to decrease towards the nearly constant value taken by the $\frac{3}{2}0 \rightarrow \frac{3}{2}2$ transition cross section, at large energies. From these observations, there is no doubt that the effect on the cross sections of opening a new electronic rotational channel is related to temporary rotational transitions during the collision. This is quite possible because additional potential energy is available during the collision owing to attractive potential energy curves (potential well depths of about 0.08 eV are seen, for example, in Fig. 4 for the symmetry group C_{2v}); and it may be favored at low energies by orbiting in the potential wells. In particular, it has been mentioned elsewhere[19] that coupling with closed rotational channel may be important in low-energy collisions. Closed channels have not been included in the present calculations, causing the sudden variations with E_R in some cross sections when a new electronic rotational channel is open. Consideration of the closed channels in the calculations are thought to smooth somewhat these sudden changes in the cross sections. However, for relative collision energies E larger than 0.1 eV the closed channels are expected to be unimportant, and convergence in the cross sections should have been reached.

In view of the results reported in Figs. 12–15 and Tables I and II, general remarks can be made, except in the low-energy region where the structure in the cross sections results from rather intricate mechanisms. We first consider the case of H_2 (Figs. 12 and 13 and Table I). With regard to the same type of inelasticity [excitation, deexcitation, or near-resonant process, as defined by ΔE in reaction (1)], the magnitudes of the cross sections for electronic-to-rotational transitions $\frac{1}{2}j_2 \rightarrow \frac{3}{2}j_2'$ decrease generally with increasing values of $|\Delta E|$. Considering separately para-H_2 or ortho-H_2, the magnitudes of the cross sections for the $\frac{1}{2}j_2 \rightarrow \frac{3}{2}j_2$ transitions are the smallest for $j_2=0$ or 1; they are seen to take comparable values for $j_2=2$, 4, and 3 at $E_R \gtrsim 0.1$ eV. In general, one finds that the cross section for an excitation process is an increasing function of E_R; the cross section for a deexcitation process increases rapidly at low energies and then decreases towards a nearly constant value at large energies E_R. In the case of Rb-D_2 collisions there are some deviations to these rules because of near-resonant transitions: $\Delta E=0.0072$ eV for the $\frac{1}{2}2 \rightarrow \frac{3}{2}0$ transition and $\Delta E=-0.0076$ eV for the $\frac{1}{2}3 \rightarrow \frac{3}{2}1$ transition. Thus the cross section for the $\frac{1}{2}2 \rightarrow \frac{3}{2}0$ transition reaches values as large as about 21 $Å^2$ at low energies ($E_R \simeq 0.07$–0.10 eV) and then decreases with E_R; the cross section for the $\frac{1}{2}3 \rightarrow \frac{3}{2}1$ transition (deexcitation process) increases abruptly at low energies up to about 17 $Å^2$, exhibits a structure due to the opening of the $|\frac{3}{2}3\rangle$ channel in the close-coupling calculations, and then increases slowly at large values of E_R. The cross section for the $\frac{1}{2}0 \rightarrow \frac{3}{2}0$ transition takes abnormally smaller values than the one for the $\frac{1}{2}0 \rightarrow \frac{3}{2}2$ transition, in spite of the larger energy splitting involved in the latter transition. In contrast also with the Rb + H_2 collisions, the cross section for the $\frac{1}{2}1 \rightarrow \frac{3}{2}1$ transition does not increase with E_R but takes nearly constant values for $E_R \gtrsim 0.07$ eV. Comparing the results obtained for H_2 and D_2, the enhancement of the cross sections corresponding to the near-resonant transitions is clearly observed at low energies; but for $E_R \gtrsim 0.1$ eV, some transition cross sections in the case of Rb + H_2 collisions are seen to take values as large as those taken by the cross sections for the near-resonant transitions in Rb + D_2 collisions.

In order to estimate the importance of coupling mechanisms involved during the Rb + H_2,D_2 collisions, the probabilities $P_{j_1'j_2' \leftarrow j_1j_2}(E,b)$ as defined by Eqs. (7) and (8) have been drawn versus the impact parameter b for the most important transitions, and for each Rb + ortho- or para-M system (see Figs. 19–24). For comparison between the Rb + H_2,D_2 collisions, typical relative collision energies E (referring to the $\frac{1}{2}$ 0 or $\frac{1}{2}$ 1 level) have been considered, which are twice larger for H_2 than for D_2 to take into account the difference of masses. It is striking to see that most of the probabilities are practically zero for $b>8$ a.u., indicating that the nonadiabatic radial coupling $d_{12}^{(R)}(R,\gamma)$ contributes much to processes (1). In the case of the $\frac{1}{2}2 \rightarrow \frac{3}{2}0$ and

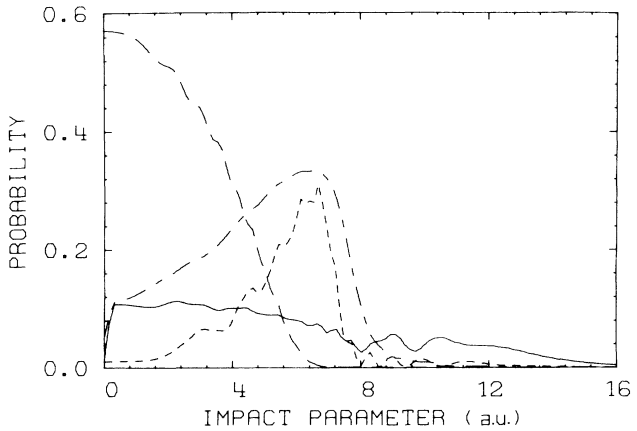

FIG. 19. Probabilities vs the impact parameter [as defined in Eqs. (7) and (8)] for various transitions in $Rb(5\,^2P_{j_1})$ + para-$H_2(j_2)$ collisions, at $E=0.205$ eV: $\frac{1}{2}\,0\rightarrow\frac{3}{2}\,0$ (short-dashed line), $\frac{1}{2}\,0\rightarrow\frac{3}{2}\,2$ (long-dashed line), $\frac{1}{2}\,2\rightarrow\frac{3}{2}\,0$ (solid line), $\frac{1}{2}\,2\rightarrow\frac{3}{2}\,2$ (long-short-dashed line).

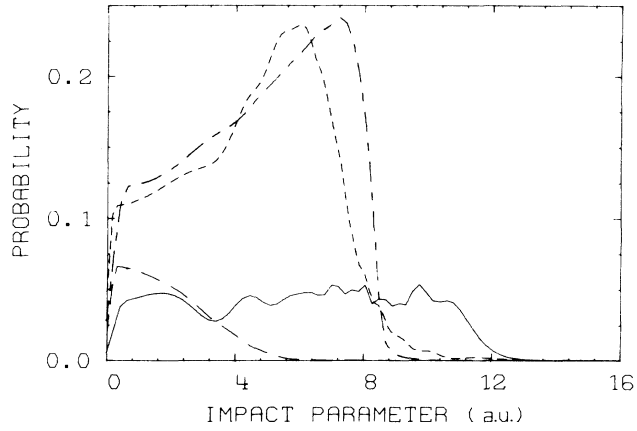

FIG. 20. Probabilities vs the impact parameter for various transitions in $Rb(5\,^2P_{j_1})$+ortho-$H_2(j_2)$ collisions, at $E=0.16$ eV: $\frac{1}{2}\,1\rightarrow\frac{3}{2}\,1$ (short-dashed line), $\frac{1}{2}\,1\rightarrow\frac{3}{2}\,3$ (long-dashed line), $\frac{1}{2}\,3\rightarrow\frac{3}{2}\,1$ (solid line), $\frac{1}{2}\,3\rightarrow\frac{3}{2}\,3$ (long-short-dashed line).

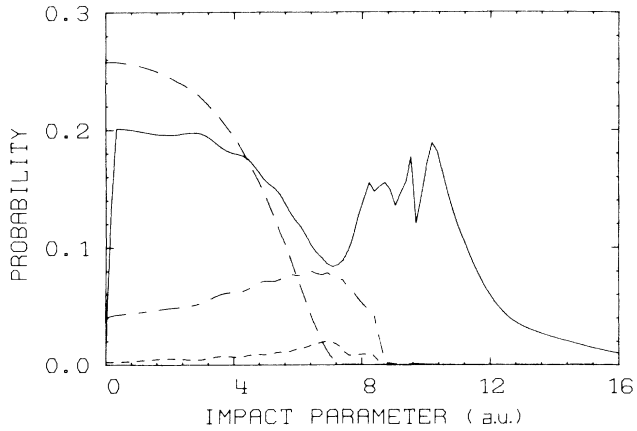

FIG. 21. Probabilities vs the impact parameter for various transitions in $Rb(5\,^2P_{j_1})$+ortho-$D_2(j_2)$ collisions, at $E=0.095$ eV, as in Fig. 19.

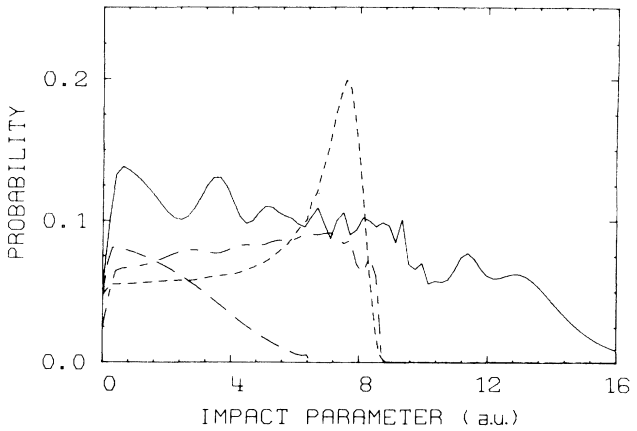

FIG. 22. Probabilities vs the impact parameter for various transitions in $Rb(5\,^2P_{j_1})$+para-$D_2(j_2)$ collisions, at $E=0.085$ eV, as in Fig. 20.

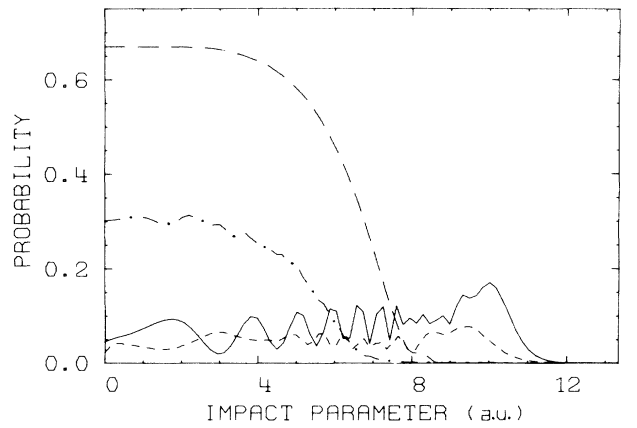

FIG. 23. Probabilities vs the impact parameter for rotational transitions in $Rb(5\,^2P_{j_1})+H_2,D_2$ collisions ($E=0.205$ eV for para-H_2 and $E=0.095$ eV for ortho-D_2). Dash-dotted line (H_2) and long-dashed line (D_2), $\frac{1}{2}\,0\rightarrow\frac{1}{2}\,2$; short-dashed line ($H_2$) and solid line ($D_2$), $\frac{3}{2}\,0\rightarrow\frac{3}{2}\,2$.

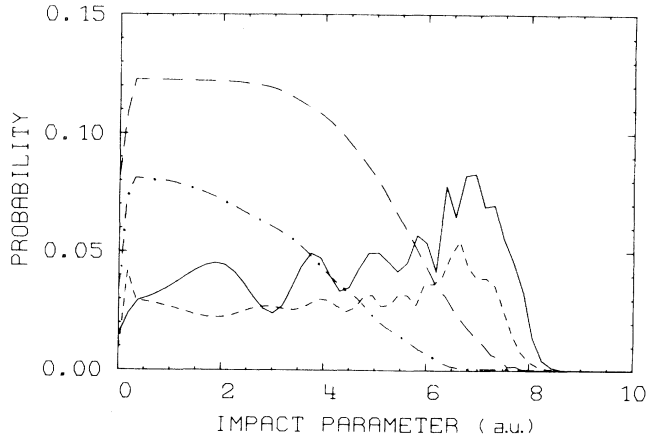

FIG. 24. Probabilities vs the impact parameter for rotational transitions in $Rb(5\,^2P_{j_1})+H_2,D_2$ collisions ($E=0.16$ eV for ortho-H_2 and $E=0.085$ eV for para-D_2). Dash-dotted line (H_2) and long-dashed line (D_2), $\frac{1}{2}\,1\rightarrow\frac{1}{2}\,3$; short-dashed line ($H_2$) and solid line ($D_2$), $\frac{3}{2}\,1\rightarrow\frac{3}{2}\,3$.

TABLE I. Cross sections (in Å^2) for the $\frac{1}{2}j_2 \rightarrow \frac{3}{2}j_2'$ transitions in Rb + H_2 collisions involving the rotational level 4 vs the relative collision energy (in eV) referring to the initial channel. The rotational transitions $j_2 \rightarrow j_2'$ are indicated in the table as well as the energy defect ΔE (in parentheses) of the electronic-to-rotational transitions. Numbers in square brackets are powers of ten, e.g., $7.47[-7] = 7.47 \times 10^{-7}$.

	Rotational transition and ΔE				
	$0 \rightarrow 4$	$2 \rightarrow 4$	$4 \rightarrow 0$	$4 \rightarrow 2$	$4 \rightarrow 4$
Energy	(0.177)	(0.132)	(−0.118)	(−0.074)	(0.029)
0.009			7.47[−7]	1.71[−2]	
0.054			6.64[−2]	5.96[0]	1.23[1]
0.160		6.59[−2]	7.38[−2]	4.17[0]	1.57[1]
0.205	1.05[−3]				
0.266		2.28[−1]			
0.311	1.04[−2]				

TABLE II. Cross sections (in Å^2) for the $\frac{1}{2}j_2 \rightarrow \frac{3}{2}j_2'$ transitions in Rb + D_2 collisions involving the rotational level 4 vs the relative collision energy (in eV) referring to the initial channel. Notation as in Table I.

	Rotational transition and ΔE				
	$0 \rightarrow 4$	$2 \rightarrow 4$	$4 \rightarrow 0$	$4 \rightarrow 2$	$4 \rightarrow 4$
Energy	(0.104)	(0.081)	(−0.045)	(−0.022)	(0.029)
0.0096			4.96[−4]	4.09[0]	
0.020			6.96[−3]	8.08[0]	
0.033			7.29[−1]	1.73[1]	2.00[0]
0.045			6.04[−1]	1.42[1]	5.34[0]
0.085		9.92[−2]	4.73[−1]	1.02[1]	7.88[0]
0.097		1.90[−1]			
0.108	4.43[−4]				
0.120	1.94[−3]				
0.125			4.35[−1]	8.57[0]	9.05[0]
0.137		3.65[−1]			
0.160	6.28[−3]				
0.177		5.44[−1]			
0.200	1.40[−2]				

TABLE III. Cross sections (in Å_2) for the inelastic rotational transitions $j_1 j_2 \rightarrow j_1 j_2'$ in Rb + H_2 collisions involving the rotational level 4 vs the relative collision energy (in eV) referring to the initial channel. The energy defect ΔE of the inelastic rotational transition $j_2 \rightarrow j_2'$ is indicated in parentheses.

	Transition and ΔE			
	$\frac{1}{2}0 \rightarrow \frac{1}{2}4$	$\frac{1}{2}2 \rightarrow \frac{1}{2}4$	$\frac{3}{2}0 \rightarrow \frac{3}{2}4$	$\frac{3}{2}2 \rightarrow \frac{3}{2}4$
Energy	(0.147)	(0.103)	(0.147)	(0.103)
0.115		7.87[−4]		
0.130				7.06[−1]
0.160	1.55[−7]	6.59[−2]		
0.176			5.76[−2]	
0.205	6.27[−3]			
0.236				9.34[−1]
0.266		8.13[−1]		
0.281			2.51[−2]	
0.311	3.45[−2]			

TABLE IV. Cross sections (in Å^2) for the inelastic rotational transitions $j_1 j_2 \rightarrow j_1 j_2'$ in Rb + D_2 collisions involving the rotational level 4 vs the relative collision energy referring to the initial channel. Notation as in Table III.

	Transition and ΔE			
Energy	$\frac{1}{2}0\rightarrow\frac{1}{2}4$ (0.074)	$\frac{1}{2}2\rightarrow\frac{1}{2}4$ (0.052)	$\frac{3}{2}0\rightarrow\frac{3}{2}4$ (0.74)	$\frac{3}{2}2\rightarrow\frac{3}{2}4$ (0.052)
0.056				8.26[−1]
0.068				1.68[0]
0.072		1.76[−4]		
0.079			2.90[−2]	
0.085	8.06[−7]	1.49[0]		
0.091			7.49[−2]	
0.097		1.62[0]		
0.108	5.65[−2]			2.19[0]
0.120	7.67[−2]			
0.131			1.37[−1]	
0.137		2.03[0]		
0.148				2.31[0]
0.160	1.59[−1]		1.93[−1]	
0.177		2.36[0]		
0.200	2.40[−1]			

$\frac{1}{2}3\rightarrow\frac{3}{2}1$ transitions, however, the probabilities may take significant values up to $b\simeq 16$ a.u., indicating that the radial coupling $d_{13}^{(R)}(R,\gamma)$ contributes also to the transitions. In particular, for the Rb-D_2 collisions where these transitions are near resonant, this coupling mechanism seems to be dominant. This result appears to be consistent with the fact that for $A(n\,^2P)+M$ collisions with $A(n\,^2P)$ fine-structure energy splittings much smaller than for Rb($5\,^2P$), no significant isotopic effect has been observed and no large differences in the cross sections have been found when He is taken as the perturber instead of H_2 (see, for example, Refs. 8 and 9). It is also consistent with previous conclusions of Hickman[14] when comparing his results for Rb($5\,^2P$)+H_2 and K($4\,^2P$)+H_2 collisions. The fact that impact parameters as large as $b\simeq 16$ a.u. contribute to the $\frac{1}{2}2\rightarrow\frac{3}{2}0$ and $\frac{1}{2}3\rightarrow\frac{3}{2}1$ transition probabilities in the case of D_2 indicates that other nonadiabatic coupling such as $d_{23}^{(R)}(R,\gamma)$ or $d_{23}^{(\gamma)}(R,\gamma)$ may participate to the transitions. Finally, the probabilities for the inelastic rotational transitions $j_1 j_2\rightarrow j_1 j_2'\neq j_2$ take larger values in the case of D_2 than for H_2 (see Figs. 23 and 24), showing the important role played by the rotational levels for near-resonant transitions. It should be noted that for D_2 as well as for H_2 the probabilities for the $\frac{3}{2}0\rightarrow\frac{3}{2}2$ and $\frac{3}{2}1\rightarrow\frac{3}{2}3$ rotational transitions take their largest values at relatively large values of b (up to $b\simeq 12$ a.u. for the $\frac{3}{2}0\rightarrow\frac{3}{2}2$ transition) in contrast with the probabilities for the $\frac{1}{2}0\rightarrow\frac{1}{2}2$ and $\frac{1}{2}1\rightarrow\frac{1}{2}3$ transitions. The particular role played by the $\frac{3}{2}j_2$ levels has been previously noted when discussing the sudden variations with E_R of the cross sections as a new electronic rotational channel is included in the close-coupling calculations. Thus, the above remarks substantiate the conclusion that the rotational levels of the molecule play an important role in Rb($5\,^2P$)+M collisions, even in the case where nonresonant processes are considered. This is also clearly illustrated by the comparisons between experimental[10] and calculated cross sections concerning the $5\,^2P_{1/2}\rightarrow 5\,^2P_{3/2}$ fine-structure in Rb, as reported in the following.

The cross section for the fine-structure transition $5\,^2P_{1/2}\rightarrow 5\,^2P_{3/2}$ in Rb induced by collisions with H_2 and D_2 can be evaluated from the cross sections for the individual electronic-to-rotational transitions previously reported and given a rotational population distribution of the molecule. As in the crossed-beam experiment of Cuvellier *et al.*,[10] we have assumed the populations of the rotational levels of the molecule to be in thermodynamic equilibrium at a temperature $T_{\rm rot}$. This assumption is well justified for the rotational levels representing individually more than 5% of the total population, that is, $j_2=0,1,2$. The comparisons between the present results and the experimental data[10] are reported in Figs. 25 and 26, respectively, for H_2 and D_2. It is to be noted that the present results have been obtained considering the mean energy of each relative collision energy range experimentally investigated. It should be pointed out that the experimental cross sections have been determined in absolute values with an estimated uncertainty of about 20%.[10] The agreement between experiment and theory is seen to be very good for the dependences of the cross sections with E and $T_{\rm rot}$, as well as for the absolute values of the cross sections. A discussion of these results may be found in our earlier paper.[22] In this paper we would like to emphasize the importance of the rotational population of the levels. For this purpose, we have reported in Figs. 25 and 26 the individual contributions $\omega(j_2,T_{\rm rot})\sigma_{3/2\leftarrow 1/2\,j_2}(E)$ of the rotational levels to the total fine-structure transition cross section, where $\sigma_{3/2\leftarrow 1/2\,j_2}(E)=\sum_{j_2'}\sigma_{3/2\,j_2'\leftarrow 1/2\,j_2}(E)$ and $\omega(j_2,T_{\rm rot})$ is the population weight of the rotational level j_2 at the temperature $T_{\rm rot}$. The major role played by the rotational level $j_2=2$ of D_2 is clearly seen in Fig. 26 to explain qualitatively the dependence with $T_{\rm rot}$ of the fine-

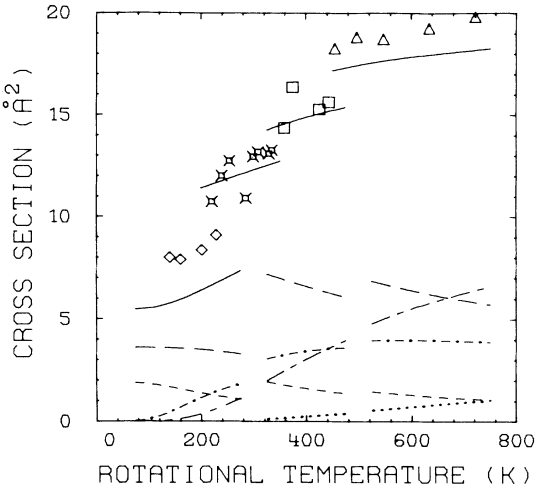

FIG. 25. Comparisons between the experimental (Ref. 10) (symbols) and the calculated (solid lines) cross sections for the $5\,^2P_{1/2}\rightarrow 5\,^2P_{3/2}$ transition in Rb + H_2 collisions vs the H_2 rotational temperature, and for various relative energy ranges experimentally investigated: ◇, $E=0.07$–0.08 eV; ⌑, $E=0.11$–0.13 eV; □, $E=0.15$–0.17 eV; and Δ, $E=0.20$–0.21 eV. The calculated cross sections correspond to the mean energy of each energy range. The calculated contributions of the various rotational levels of H_2 to the fine-structure transition are also shown for $E=0.075$, 0.16, and 0.205 eV: $\frac{1}{2}0\rightarrow\frac{3}{2}$ (short-dashed line), $\frac{1}{2}2\rightarrow\frac{3}{2}$ (dash-dotted line), $\frac{1}{2}4\rightarrow\frac{3}{2}$ (dotted line), $\frac{1}{2}1\rightarrow\frac{3}{2}$ (long-dashed line), and $\frac{1}{2}3\rightarrow\frac{3}{2}$ (long-short-dashed line).

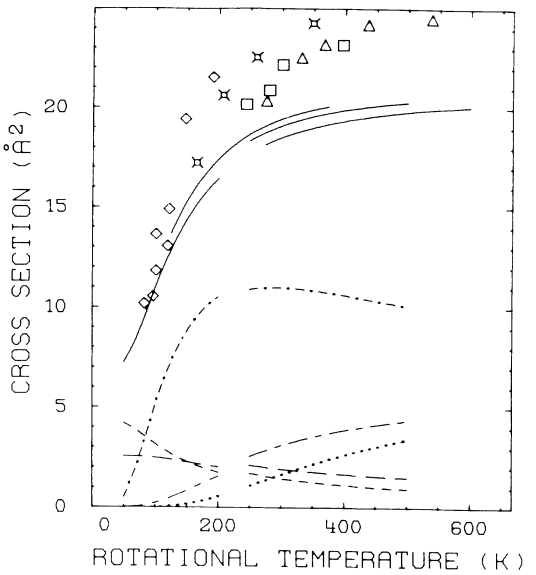

FIG. 26. Comparisons between the experimental (Ref. 10) (symbols) and the calculated (solid lines) cross sections for the $5\,^2P_{1/2}\rightarrow 5\,^2P_{3/2}$ transition in Rb + D_2 collisions vs the D_2 rotational temperature, and for various relative energy ranges: ◇, $E=0.08$–0.09 eV; ⌑, $E=0.12$ eV; □, $E=0.15$–0.17 eV; △, $E=0.20$–0.21 eV. The calculated contributions of the various rotational levels of D_2 to the fine-structure transition are also shown, as in Fig. 25, for the mean relative energies $E=0.085$ and 0.16 eV.

structure transition cross section, in agreement with the conclusions of Cuvellier *et al.*[10] But our results show clearly that the other rotational levels are necessary to reproduce the behavior of the experimental cross sections in absolute values. In particular, considering the results reported in Fig. 26 and those concerning the cross sections $\sigma_{3/2\leftarrow 1/2\,j_2}(E)$ which have been previously reported,[22] it may be seen that the effect of the quasiresonance for the $\frac{1}{2}2\rightarrow\frac{3}{2}0$ transition has been amplified by a large population of the rotational level $j_2=2$ of D_2, at low temperatures $T_{\rm rot}$. As clearly seen in Fig. 25 for H_2, it is a fine balance between the importance of the individual fine-structure transitions from the various rotational levels j_2 and the rotational population distribution which determines the very good agreement between experiment and theory. At low temperature $T_{\rm rot}$, or low relative energies E, this agreement might be improved if closed rotational channels are considered in the close-coupling calculations as previously discussed. In the case of D_2, the slight departure of the calculated cross sections from the experimental data could be removed by including the rotational levels $j_2=5$ and 6 in the close-coupling calculations. Indeed, these rotational levels becomes appreciably populated for $T_{\rm rot}\gtrsim 400$ K for both H_2 and D_2, but for D_2 the rotational levels are much closer to each other than for H_2 (see Fig. 18). Therefore, the rotational levels $j_2=5$ and 6 should be involved in the close-coupling calculations for $E\gtrsim 0.15$ eV in the case of D_2.

IV. CONCLUSION

Three-dimensional close-coupling quantum-mechanical calculations have been performed for thermal to suprathermal Rb($5\,^2P_{j_1}$)+para- or ortho-$M(j_2)$ collisions, where $M\equiv H_2$ or D_2, and the total cross sections for all the inelastic level-to-level transitions $j_1j_2\rightarrow j_1'j_2'$ have been determined. The calculations are shown to use implicitly realistic adiabatic potential surfaces which have been determined from previous l-dependent pseudopotential molecular structure calculations. These potential energy surfaces are then used for evaluating the main nonadiabatic coupling matrix elements which are involved during the collision. The present study concludes that two main nonadiabatic coupling mechanisms are in competition for inducing fine-structure transitions: There are radial coupling terms which result from spin-orbit decoupling during the collision, and which are well located at short ($R\lesssim 8$ a.u.) and intermediate ($R\simeq 12$–15 a.u.) distances. These conclusions are in agreement with a previous study of Rb($n\,^2P$)+H_2 collisions by Hickman,[13,14] where a two-dimensional semiclassical model was developed. Hickman's model treated H_2 as a structureless particle, therefore leading to a neglect of the rotational levels of the molecule. The present study shows clearly that the rotational levels of the molecule play an important role during the collision, for D_2 as well as for H_2. In particular it is shown that close-coupling calculations including the rotational levels of H_2 and D_2 are necessary for correctly interpreting the crossed-beam measurements of Cuvellier *et al.*[10] con-

cerning the $5\,^2P_{1/2} \rightarrow 5\,^2P_{3/2}$ transition in Rb. The calculated cross sections for the fine-structure transition are shown to result from a fine balance between the relative importance of the $\frac{1}{2} j_2 \rightarrow \frac{3}{2}$ transition cross sections, as well as their energy dependences, and the relative population of the rotational levels. Thus the strong isotopic effect which was experimentally observed can be fully understood. These conclusions are not specific to the present study but should be kept in mind when interpreting this type of experimental data (see, for example, Ref. 32). The very good agreement which has been obtained between experiment and theory provides also a strong support of our previous l-dependent pseudopotential molecular structure calculations,[21] since it has been shown that the total cross sections reported in this paper are not only sensitive to the intermediate range potentials ($R \simeq 10-15$ a.u.) but also to the short range potentials ($R \lesssim 8$ a.u.). Therefore, it should be interesting to use these potential surfaces in more detailed studies of fine-structure transitions (i.e., differential cross sections or polarization effects). They should be used also to investigate some intermultiplet transitions for which the general formulation of Ref. 20 is applicable. Finally, it is hoped that the present work will stimulate more detailed experimental studies of the type of processes considered in this paper.

ACKNOWLEDGMENTS

J. Pascale and F. Rossi wish to thank Professor J. Baudon for helpful and stimulating discussions. J. Pascale is also indebted to Dr. J.-M. Launay for a discussion of the role of closed channels in close-coupling calculations.

---

*On leave from the Department of Physics, University of Windsor, Ontario, Canada N9B 3P4.

[1]W. H. Breckenridge and H. Umemoto, in *The Dynamics of the Excited State,* edited by K. Lawley (Wiley, New York, 1982), p. 325.

[2]I. V. Hertel, in *The Dynamics of the Excited State,* edited by K. Lawley (Wiley, New York, 1982), p. 475.

[3]J. C. Tully, J. Chem. Phys. **59**, 5122 (1973).

[4]N. C. Blais, D. G. Truhlar, and B. C. Garrett, J. Chem. Phys. **78**, 2956 (1983), and references therein.

[5]N. C. Blais and D. G. Truhlar, J. Chem. Phys. **79**, 1334 (1983).

[6]E. S. Hrycysshyn and L. Krause, Can. J. Phys. **48**, 2761 (1970).

[7]W. E. Baylis, E. Walentynowicz, R. A. Phaneuf, and L. Krause, Phys. Rev. Lett. **31**, 741 (1973).

[8]J. Elward-Berry and M. J. Berry, J. Chem. Phys. **72**, 4510 (1980).

[9]J. M. Mestdagh, J. Berlande, J. Cuvellier, P. de Pujo, and A. Binet, J. Phys. B **15**, 439 (1982).

[10]J. Cuvellier, J. M. Mestdagh, M. Ferray, and P. de Pujo, J. Chem. Phys. **79**, 2848 (1983).

[11]R. W. Berends, P. Skalinski, and L. Krause, J. Chem. Phys. B **17**, 605 (1984).

[12]B. Amae and C. Bottcher, J. Phys. B **11**, 1249 (1978).

[13]A. P. Hickman, Phys. Rev. Lett. **47**, 1585 (1981).

[14]A. P. Hickman, J. Phys. B **15**, 3005 (1982).

[15]F. Rossi, Thèse d'Etat, Université de Paris–Nord, 1986.

[16]E. E. Nikitin, Adv. Chem. Phys. **28**, 317 (1975).

[17]F. Rebentrost and A. Lester, Jr., J. Chem. Phys. **67**, 3367 (1977).

[18]F. Rebentrost, Chem. Phys. Lett. **58**, 18 (1978).

[19]D. R. Flower and J.-M. Launay, J. Phys. B **10**, 3673 (1977).

[20]W. E. Baylis, J. Pascale, and F. Rossi, preceding paper, Phys. Rev. A **36**, 4212 (1987).

[21]F. Rossi and J. Pascale, Phys. Rev. A **32**, 2657 (1985).

[22]J. Pascale, F. Rossi, and W. E. Baylis, Europhys. Lett. **3**, 183 (1987).

[23]R. H. G. Reid, J. Phys. B **6**, 2018 (1973) and references therein.

[24]A. Messiah, *Mécanique Quantique* (Dunod, Paris, 1972), Vol. 2.

[25]B. R. Johnson, J. Comput. Phys. **13**, 445 (1973).

[26]D. R. Flower and J.-M. Launay, J. Phys. B **10**, L229 (1977).

[27]L. D. Landau and E. M. Lifshitz, *Quantum Mechanics* (Pergamon, London, 1958), Vol. 2, p. 262.

[28]D. G. Truhlar, J. W. Duff, N. C. Blais, J. C. Tully, and B. C. Garrett, J. Chem. Phys. **77**, 764 (1982).

[29]J. C. Tully, J. Chem. Phys. **59**, 5122 (1973).

[30]J. Pascale, in *Proceedings of the Thirteenth Summer School on Quantum Optics,* edited by J. Fiutak and J. Mizerski (World Scientific, Singapore, 1986), p. 71.

[31]G. Herzberg and K. P. Huber, in Constants of Diatomic Molecules (Van Nostrand Reinhold, New York, 1979), Vol. IV.

[32]H. J. Yuh and P. J. Dagdigian, J. Phys. B **17**, 4351 (1984).